ACS Catalysis

Research Article

pubs.acs.org/acscatalysis

Effects of Li Doping on MgO-Supported Sm_2O_3 and TbO_x Catalysts in the Oxidative Coupling of Methane

Trenton W. Elkins,[†] Björn Neumann,[‡] Marcus Bäumer,[‡] and Helena E. Hagelin-Weaver*,[†]

[†]Department of Chemical Engineering, University of Florida, Gainesville, Florida 32611, United States

[‡]Institute of Applied and Physical Chemistry & Center for Environmental Research and Sustainable Technology, University Bremen, Leobener Strasse UFT, 28359 Bremen, Germany

ABSTRACT: Rare earth oxides (REOs), particularly the sesquioxides, such as Sm_2O_3 and La_2O_3, have been investigated as promising catalysts in the oxidative coupling of methane (OCM). Much less attention has been paid to the reducible REOs because they are expected to give oxidation products, such as CO and CO_2 (CO_x), rather than the desirable ethane and ethylene (C_{2+}). Because Li addition can improve the performance of Sm_2O_3 in the OCM reaction and Li/MgO is commonly used as a reference OCM catalyst, the effects of lithium addition to a reducible oxide, TbO_x, were investigated in detail in this study and compared with a Sm_2O_3 catalyst, which is the best single component OCM catalyst. Because of the well-documented volatility of lithium under OCM conditions, particularly for the Li/MgO system, the stability of lithium-doped samaria and terbia catalysts was examined as a function of preparation methods in this study. As expected, terbia supported on nanoparticle magnesia (n-MgO) is not a very active or selective OCM catalyst, and most of the observed selectivity toward C_{2+} products is likely due to the n-MgO support. In contrast, Li-doped TbO_x/n-MgO prepared using a coimpregnation method yields a highly active and selective catalyst. The Li-TbO_x/n-MgO catalyst yields the same methane conversion as pure Sm_2O_3, and has a higher C_{2+} selectivity than the Li-Sm_2O_3/n-MgO catalyst. The stability of the Li-TbO_x/n-MgO catalyst is also higher than that of the Li-Sm_2O_3/n-MgO catalyst, and the loss of activity for the lithium-doped terbia catalyst appears to be the same as for the undoped Sm_2O_3/n-MgO catalyst (and undoped TbO_x/n-MgO). The characterization data indicate stronger interactions between Li and TbO_x than between Li and Sm_2O_3, which may explain the higher stability of the Li-TbO_x/n-MgO catalysts. There are also indications that Li enters the TbO_x lattice and reduces $TbO_{1.81}$, to Tb_2O_3 during reaction, which can explain the higher C_{2+} selectivity compared with undoped TbO_x/n-MgO. Furthermore, the Li-TbO_x/n-MgO catalyst in this study is active at lower temperatures (600−700 °C) than typically used in the OCM (around 800 °C). Therefore, the Li-TbO_x/n-MgO catalysts have potential to be very effective OCM catalysts, even though undoped TbO_x/n-MgO catalysts are more selective toward CO_x than C_{2+} products.

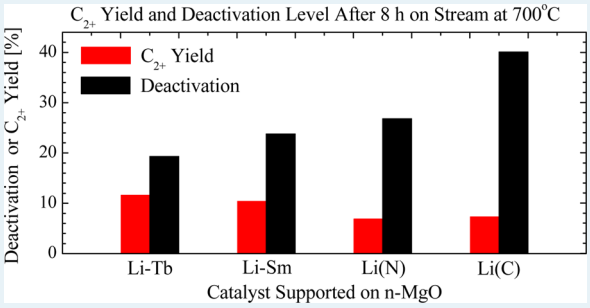

KEYWORDS: *oxidative coupling of methane, samarium oxide, terbium oxide, lithium doping, magnesium oxide support, XPS, XRD, DRIFTS*

1. INTRODUCTION

The oxidative coupling of methane (OCM) has been extensively studied over the past few decades since the initial work of Keller and Bhasin.[1] Ethylene, one of the two C_2 hydrocarbon products in OCM, is a highly valuable feedstock material for synthesizing longer chain hydrocarbons, polymers, and other products. Early work in the OCM field found that doping a magnesium oxide support with lithium produces an active catalyst under OCM conditions with a relatively high C_2 product selectivity.[2,3] This catalyst system has since been a reference system in many studies due to its activity, selectivity, and simplicity. However, lithium is volatile under OCM reaction conditions, which is detrimental to the catalyst's long-term stability, and it has been found that within the first few hours of reaction, the majority of the lithium will leave the surface of the catalyst, resulting in a sharp decrease in activity.[4,5] The underlying issue has been attributed to the low solubility of lithium in the magnesium oxide lattice together with the volatility of LiOH at the high reaction temperature.[6]

In addition to Li-MgO, a large number of catalysts with different compositions have been investigated in the oxidative coupling of methane.[7−31] The best-performing catalyst to date is the complex, multicomponent Mn-Na_2WO_4/SiO_2 catalyst because of its high activity and long-term stability in multiple reactor types.[28−31] However, this catalyst requires temperatures in excess of 800 °C for optimum activity and selectivity.[31] Among the highest performing single-component OCM catalysts are rare-earth oxides (REOs) in the lanthanide series, particularly Sm_2O_3.[16−24] In general, sesquioxides, such as Sm_2O_3 and La_2O_3, which do not form higher oxides, are the

Received: January 31, 2014
Revised: April 21, 2014
Published: April 25, 2014

   dx.doi.org/10.1021/cs500138j | ACS Catal. 2014, 4, 1972−1990

most effective in selectively promoting CH_4 coupling to ethane and ethylene,[22] and reducible REOs (e.g. CeO_2, Tb_4O_7, Pr_6O_{11}) are selective only after doping with, for example, alkali metals.[27,32] Addition of alkali and alkaline-earth metals to Sm_2O_3, and other nonreducible REOs, such as La_2O_3, has proven to be beneficial to the system's C_2 yield,[26] but the activity (i.e. CH_4 conversion) can be negatively influenced under certain reaction conditions.[26,33] Furthermore, deactivation issues similar to the Li/MgO have been noted, particularly for the Li-doped catalysts. Although reducible REOs doped with alkali and alkaline earth metals have appeared in the literature, no systematic investigation is available on how the lithium influences the REO catalyst and if the effects are dependent on the specific REO used. Furthermore, very few studies using terbium oxide as the active component are available in the literature,[20,26,27] even though there are indications that terbia-based OCM catalysts can benefit greatly from alkali doping.[27]

For these reasons, it was decided to investigate the effects of Li doping on both Sm_2O_3 and TbO_x to determine if the effects of Li are different over the two catalysts and if it is possible to prepare a highly active TbO_x-based catalyst with activity below 800 °C. Because the activity and selectivity can be dependent on catalyst preparation methods and catalyst precursors, three different preparation methods were examined: a microemulsion-assisted, precipitation-deposition method and an incipient wetness impregnation method in which the lithium was added either with the rare earth oxide precursor (coimpregnation) or after the impregnation with the rare earth oxide (sequential impregnation). The effect of the lithium precursor was also explored using lithium nitrate and lithium chloride. Although we have shown previously that a 20% samaria loading on an alumina support can be an active catalyst in OCM,[25] the focus in this study was on a more conventional OCM support, that is, magnesia, to enhance the C_{2+} yield compared with the alumina-supported catalysts. Furthermore, this choice of support facilitates comparisons with Li/MgO, which is a commonly used OCM catalyst.

2. EXPERIMENTAL SECTION

2.1. Catalyst Preparation. *2.1.1. Rare-Earth Oxide-Based Catalysts via Incipient Wetness Impregnation.* Samaria- and terbia-based catalysts were synthesized via incipient wetness impregnation (IWI) onto a low-surface-area (20.4 m^2/g) nanoparticle magnesium oxide support (n-MgO received from NanoScale Materials Inc.[34]) using an aqueous solution of the REO precursor (samarium(III) nitrate hydrate or terbium(III) nitrate hydrate, 99.9% REO, Alfa Aesar). Briefly, an appropriate amount of the REO precursor was dissolved into a volume of DI water equal to the volume of the pores of the support. The solution was then added dropwise to the support under continuous stirring until incipient wetness. The resulting catalysts were dried at 80 °C for 3 h and overnight at 105 °C before calcination at 800 °C for 4 h. A lithium nitrate ($LiNO_3$ hydrate, Puratronic, 99.999% metal basis) or lithium chloride ($LiCl_3$ hydrate, Puratronic, 99.998%) precursor was also added to the REO precursor solution for preparation of coimpregnated lithium-doped samples. For the sequential impregnation, the REO precursor was first added to the support, and the lithium precursor was added after drying. The weight percentage of the REOs was always 20% (metal oxide basis), and the lithium loading was 2.5%, resulting in catalyst compositions of 20/80 REO/n-MgO and 2.5/20/77.5 Li-REO/n-MgO for undoped and lithium-doped catalysts, respectively.

2.1.2. Rare-Earth Oxide Catalysts via Microemulsion Method. Samaria- and terbia-based catalysts were also synthesized via a reverse micelle, water in toluene, microemulsion method using n-MgO as the support material. The procedure has been implemented in previous research using an aluminum oxide support.[25] Briefly, the support was suspended in 22.5 mL of DI H_2O, and the REO precursor salt was added to the aqueous solution and allowed to stir for 15 min. The aqueous phase was then added to 187 mL of toluene dropwise, and afterward, a surfactant, Tween 80 (Acros Organics), was added to the mixture dropwise (~4 mL) until emulsion formation. An aqueous phase of NaOH (50% stoichiometric excess) was added dropwise to the system to produce the rare-earth hydroxide in the aqueous phase inside the reverse micelles. The resulting mixture was allowed to stir overnight and then was centrifuged to collect the product, which was washed in a water/ethanol (50/50 vol %) solution to clean the particles. The catalysts were then dried at 105 °C overnight and calcined at 800 °C for 4 h.

2.1.3. Li/n-MgO Reference Systems Preparation. Because Li/MgO catalysts have been studied in the OCM reaction, two 2.5/97.5 Li/n-MgO reference catalysts were included in the study for comparison. One catalyst, {Li(N)/n-MgO}, was prepared using the lithium nitrate salt precursor and the same method (IWI) used to prepare the Li-doped Sm_2O_3/n-MgO and TbO_x/n-MgO catalysts. The second, {Li(C)/n-MgO}, was prepared by following a slurry method previously reported by Lunsford and co-workers.[3] This method involves slowly adding Li_2CO_3 (99.99%, Alfa Aesar) to an aqueous magnesium oxide slurry, which was then stirred under gentle heating until a paste formed. The resulting mixture was dried overnight and then calcined at 800 °C for 4 h.

2.2. Catalyst Characterization Methods. *2.2.1. Surface Area Analysis.* Brunauer–Emmett–Teller (BET) surface area measurements were performed on all catalysts using a 6-point isotherm on a Quantachrome NOVA 1200 instrument operating at liquid nitrogen temperatures. All correlation values were >0.999.

2.2.2. Electron Microscopy. Transmission electron microscopy (TEM), including energy dispersive X-ray spectroscopy (EDX), was performed using an FEI Tecnai F20 S-TWIN microscope with an operating voltage of 200 kV. TEM images were acquired with a slow-scan CCD camera with an integrated Gatan image filter, model 2001. For the preparation of the TEM grids, a small amount of each sample was suspended in acetone and ultrasonicated. Finally, a droplet (25 μL) was placed on a carbon-coated copper grid.

2.2.3. X-ray Diffraction Analysis. Powder X-ray diffraction (PXRD) data were acquired for the catalysts using a PANalytical X'Pert MPD Pro l diffractometer in Bragg–Brentano geometry. The setup was equipped with a secondary Ni filter, Cu Kα1,2 radiation and a X'Celerator multistrip detector.

2.2.4. X-ray Photoelectron Spectroscopy. Most XPS measurements were collected on a PerkinElmer 5100 XPS system using an aluminum X-ray source (fresh samples). A thin layer of catalyst was placed on double-sided carbon conductive tape for sample preparation. In all cases, samples were dried in an oven overnight at 105 °C to minimize the water adsorption on the catalyst surface. On the PerkinElmer 5100 XPS system, survey scans were collected using a time/step of 30 ms with a

dx.doi.org/10.1021/cs500138j | ACS Catal. 2014, 4, 1972–1990

0.5 eV step size and a pass energy of 89.45 eV, and the time/step was 50 ms with a step size of 0.1 eV and a pass energy of 35.75 eV for the narrow scans. Survey and narrow scan spectra were collected using a total of 10 and 50 scans, respectively. Because the spent catalysts were problematic in the ultrahigh vacuum environment as a result of excessive outgassing, one spent and one fresh catalyst were analyzed using a different XPS instrument with a lower resolution. This instrument is equipped with a double-pass, cylindrical-mirror analyzer (PHI model 25-270AR) and a Mg Kα X-ray source (PHI 04-151). Data collection was accomplished using a computer-interfaced, digital pulse-counting circuit[35] followed by smoothing with digital filtering techniques. Spectra were taken in the retarding mode with a pass energy of 50 eV for survey spectra and 25 eV for narrow scans on this instrument. For the C 1s, including the Li 1s region, 25 scans were collected; for the Tb 4d peaks, a total of 100 scans were collected to get a sufficient signal-to-noise. Samples for this system were pressed into aluminum cups before insertion into the ultrahigh vacuum chamber. Charge shift corrections were made on all samples by assuming a C 1s signal of 284.6 eV.[36] No signs of differential charging were observed in this study.

To obtain a more quantitative estimate of the contribution from different oxygen species on the surface of these catalysts, the O 1s peak was deconvoluted on selected catalysts by fitting the data using two Gaussian functions with full width at half maxima of 2.0 eV. Although there are more than two oxygen species on the surface of these catalysts (e.g. MgO, REO, and hydroxyl plus carbonate groups), it is exceedingly difficult to unambiguously separate the contributions from these oxide species on the catalysts. Therefore, the deconvolutions were done to separate contributions from MgO/REO (O 1s peaks with binding energies of ~529.3 eV) and hydroxyls/carbonates (with typical binding energies around 531.5 to 532 eV).

2.2.5. Diffuse Reflectance Infrared Spectroscopy. In situ DRIFTS were performed on a Nicolet 6700 FTIR equipped with a Praying Mantis reaction chamber apparatus. Spectra were collected using 256 scans and a resolution of 4 cm^{-1}. Potassium bromide (KBr) was used to dilute the catalyst to 10% weight. Samples were degassed in situ at 450 °C under an inert flow for 30 min prior to the experiments. Backgrounds were collected after the outgassing procedure. The catalysts were then exposed to CO_2 at 50 or 250 °C for 10 min and allowed to outgas for 5 min under a He flow before the data was collected. The spectra are presented as a percent of absorbance (i.e., an absorbance of 0% indicates no adsorbed species).

2.2.6. CO_2 Temperature-Programmed Desorption. Temperature-programmed desorption measurements after CO_2 adsorption were performed on a CHEMBET 3000 instrument. A 250 mg portion of catalyst was loaded into a quartz u-tube and was outgassed under a He flow at 800 °C for 30 min prior to CO_2 exposure at 200 °C for 30 min. After allowing physically absorbed CO_2 to outgas at 200 °C, the catalyst was heated to 800 °C at a rate of 10 °C/min. Temperature measurements were recorded by a thermocouple inside the quartz u-tube (on the outlet side), and a TCD detector measured the amount of desorbed gas.

2.3. OCM Reaction Experiments. The catalyst testing was performed on a previously reported system consisting of a quartz tube reactor with an inner diameter of 10 mm and an online gas chromatograph (GC) for product monitoring equipped with two detectors, a thermal conductivity detector (TCD) and a flame ionization detector (FID) preceded by a methanizer to convert all CO and CO_2 to CH_4.[25] Each catalyst was pelletized using a Carver pellet press, then crushed using a mortar and pestle and sieved to a size range of 180−250 μm. For loading the reactor, 0.4 g of the sieved catalyst was supported in the quartz reactor tube between two pieces of quartz wool. CH_4, O_2, and an internal standard (N_2) were fed through the system at a rate of 160 standard cm^3 (sccm) (with N_2 constant at 23.2 sccm) using three mass flow controllers (MFCs), which results in a GHSV of 2400 h^{-1}. This is the highest flow rate that will give the maximum yield under the conditions in the study. The CH_4/O_2 feed ratio was held constant at 4:1 for all experiments because this is the stoichiometric amount needed for conversion of methane to ethane and water, and it was also shown to give the highest CH_4 conversion at a reasonable C_2 selectivity in a previous study.[25] Although lower CH_4/O_2 feed ratios can give a higher methane conversion, the selectivity decreases significantly as the oxygen concentration is increased. Furthermore, because the oxidation to CO and CO_2 is more exothermic than OCM reaction pathways, issues with temperature control can arise at lower CH_4/O_2 feed ratios. For these reasons, the CH_4/O_2 feed ratio was held constant at 4:1.

Quantitative analyses of products were done using the TCD and FID peak area ratios compared with the reference N_2 (all calibration curves were linear, and regression analysis resulted in fits of ≥99.9%). The reaction temperatures reported are measured by a thermocouple supporting the catalyst bed on the effluent side of the reactor. Two methane conversions are reported in this study. The first is a "total" methane conversion (X_{CH_4}), which is calculated by the difference of the methane entering the reactor system and the unconverted methane in the reactor effluent as determined by the GC (eq 1). The second methane conversion ($X^*_{CH_4}$, eq 2) is the fraction of methane converted to CO_x and C_{2+} products (CO_2, CO, and C_2 plus C_3 products), which are the products used to determine the C_{2+} selectivity ($S_{C_{2+}}$, eq 3). The C_{2+} yield ($y_{C_{2+}}$), is calculated by multiplying the methane conversion ($X^*_{CH_4}$) and the C_{2+} selectivity ($S_{C_{2+}}$) as described in eq 4. Using the $X^*_{CH_4}$ gives a more accurate C_{2+} yield that can be obtained in the reaction, even though this is not commonly accounted for, and furthermore, the difference between the X_{CH_4} and $X^*_{CH_4}$ methane conversions appears to be mainly due to carbon deposition on the reactor walls downstream of the catalyst bed and, thus, most likely due to decomposition of the more reactive products. The difference in methane conversion is not due to significant amounts of formed oxygenates, that is, condensable byproducts because DART-MS analysis on the condensate detected only trace amounts of formic acid, too low to quantify accurately.

$$X_{CH_4} = \frac{CH_{4,in} - CH_{4,out}}{CH_{4,in}} \quad (1)$$

$$X^*_{CH_4} = \frac{[2\cdot(C_2H_6 + C_2H_4) + 3\cdot(C_3H_8) + CO + CO_2]_{out}}{CH_{4,in}} \quad (2)$$

dx.doi.org/10.1021/cs500138j | ACS Catal. 2014, 4, 1972−1990

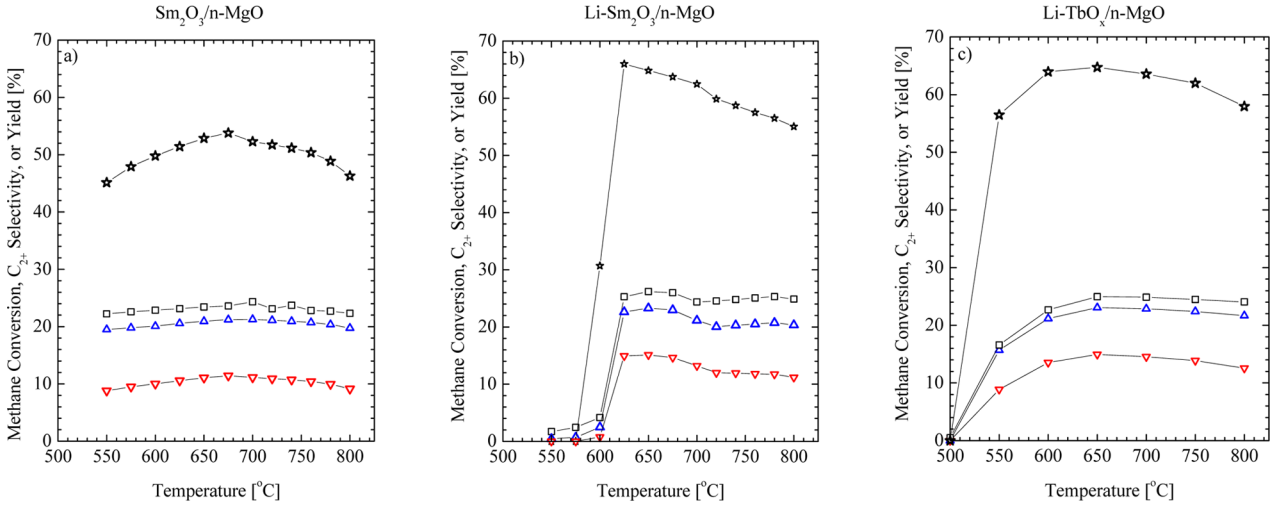

Figure 1. Reaction data during oxidative coupling of methane as a function of temperature obtained over (a) Sm_2O_3/n-MgO, (b) Li-Sm_2O_3/n-MgO, and (c) Li-TbO_x/n-MgO catalysts at a CH_4/O_2 ratio of 4:1. (□) Methane conversion (X_{CH_4}); (blue △) methane conversion to C_{2+} and CO_x products ($X^*_{CH_4}$); (☆) selectivity to C_{2+} products ($S_{C_{2+}}$); and (red ▽) C_{2+} product Yield ($Y_{C_{2+}}$).

$$S_{C_{2+}} = \frac{\text{sccm } CH_4 \text{ reacted to } C_2 \text{ and } C_3 \text{ products}}{\text{sccm } CH_4 \text{ reacted to } CO_x,\ C_2,\ \text{and } C_3 \text{ products}} \quad (3)$$

$$Y_{C_{2+}} = X^*_{CH_4} \cdot S_{C_{2+}} \quad (4)$$

The catalytic activity and selectivity were initially evaluated as a function of temperature to determine a suitable temperature interval for longer time-on-stream experiments. In an initial test reaction, product monitoring began at 300 °C, after which the temperature was increased by intervals of 100 °C until evidence of methane conversion was observed. After this experiment, a new catalyst was loaded into the reactor and brought to a temperature 100 °C lower than the activation temperature determined in the test reaction. The activity and selectivity of selected catalysts were then measured as a function of temperature by increasing the temperature in 50 °C intervals until the temperature reached 800 °C. From these experiments, two reaction temperatures (650 and 700 °C) were selected, and the OCM activity was monitored at these temperatures for 8 h. In each of these experiments (all catalysts and each reaction temperature), a new, fresh catalyst was loaded into the reactor before monitoring the reactor effluent composition. The first measurement was taken 15 min after the reactor temperature reached a steady state. Subsequent measurements were taken in 30 min intervals.

Because Li-doped catalysts are known to deactivate, the best lithium-doped catalyst was subjected to an extended 30 h reaction experiment to test the long-term stability. For the first 2 h, measurements were taken every 30 min. Afterward, the collection interval was lengthened to every hour.

3. RESULTS AND DISCUSSION

A number of Li-doped and pure REO catalysts supported on n-MgO were prepared using different methods and lithium precursors and then subjected to methane coupling experiments and catalyst characterizations to determine the effects of Li on the REO catalyst properties and if the effect is dependent on the preparation method, lithium precursor, or specific REO used.

3.1. OCM Reaction Results. *3.1.1. OCM Activity Measurements: Effects of Temperature.* To determine the best temperatures for time-on-stream experiments, the CH_4 conversion, C_{2+} selectivity, and C_{2+} product yield was monitored as a function of reaction temperature for Sm_2O_3/n-MgO, Li-Sm_2O_3/n-MgO, and Li-TbO_x/n-MgO (Figure 1). The TbO_x/n-MgO catalyst was not included in this experiment because an undoped TbO_x catalyst would be expected to be more selective toward CO and CO_2 than to C_2 products compared with the other catalysts in this study. The temperature of optimum C_{2+} product selectivity for the TbO_x/n-MgO catalyst would therefore not be as important, as for the other catalysts. As evidenced in Figure 1, the three catalysts included in the study exhibit very different behavior with reaction temperature.

The Sm_2O_3/n-MgO catalyst is surprisingly active, even at 550 °C with a CH_4 conversion of 22% and a selectivity of 44%. Similar values have been reported previously for Sm_2O_3, although for reaction temperatures of 700 °C and above.[23,37,38] In fact, the conversion and selectivity for the Sm_2O_3/n-MgO catalyst under these conditions are slightly better than those observed at a reaction temperature of 740 °C over the pure Sm_2O_3 nanoparticles in our previous study,[25] even though the rare earth oxide content is significantly lower in the n-MgO-supported catalyst. As expected,[23] increasing the temperature increases the C_{2+} selectivity, and a maximum selectivity of 53% is observed at 675 °C over this catalyst. This is also the temperature of maximum C_{2+} yield (11.4%) because the CH_4 conversion remains around 23% ± 1% in the temperature range under investigation (500−800 °C).

Doping the Sm_2O_3/n-MgO catalyst with Li improves its performance, but the catalyst requires higher temperatures to activate. Below 600 °C, very little methane is converted, and the only observed products are CO_2 with a small fraction of CO (Figure 1b). A temperature above 600 °C is required for this catalyst to exhibit a significant conversion; however, once the catalyst is activated, the activity and selectivity increase very rapidly between 600 and 625 °C. The maximum C_{2+} yield (15.1%) from the Li-Sm_2O_3/n-MgO catalyst is obtained at 650 °C, where the CH_4 conversion is 26% and the C_{2+} selectivity 65%. If the temperature is increased above 650 °C, there is a gradual decrease in selectivity while the CH_4 conversion remains around 25% ± 0.5%. The decrease in selectivity is

dx.doi.org/10.1021/cs500138j | ACS Catal. 2014, 4, 1972−1990

Table 1. Reaction Data for the Oxidative Coupling of Methane at 700 °C Obtained from MgO-Supported, Undoped and Li-Doped, Sm_2O_3 and TbO_x Catalysts

							product selectivity, %			
catalyst description[a]	Li precursor	prep. method[b]	X_{CH_4}, %[c]	$X^*_{CH_4}$, %[d]	S_{C_2}, %[e]	Y_{C_2}, %[f]	C_2H_4	C_2H_6	CO_2	CO
Sm_2O_3/n-MgO	none	IM	24.3	21.3	52.3	11.1	26.3	25.3	44.3	4.1
Sm_2O_3/n-MgO	none	ME	23.8	20.8	51.7	10.8	23.8	27.4	45.7	3.1
Li-Sm_2O_3/n-MgO-ME	$LiNO_3$	ME	25.0	21.2	63.2	13.4	38.1	23.7	34.3	3.9
LiC-Sm_2O_3/n-MgO-ME	$LiCl_3$	ME	22.5	20.4	56.2	11.5	32.3	23.0	39.5	5.2
Li-Sm_2O_3/n-MgO	$LiNO_3$	CIM	24.4	21.1	62.5	13.2	38.2	22.8	33.6	5.4
Li-Sm_2O_3/n-MgO-SIM	$LiNO_3$	SIM	26.7	20.8	61.1	12.7	38.8	21.1	32.8	7.3
LiC-Sm_2O_3/n-MgO	$LiCl_3$	CIM	25.1	22.2	58.2	12.9	33.6	23.4	39.1	3.9
LiC-Sm_2O_3/n-MgO-SIM	$LiCl_3$	SIM	24.8	22.0	61.1	12.7	31.8	27.2	37.5	3.5
TbO_x/n-MgO	none	IM	19.9	17.2	38.9	6.7	16.3	22.3	59.3	2.1
TbO_x/n-MgO-ME	none	ME	24.1	18.6	44.3	8.3	17.7	26.2	54.6	1.5
Li-TbO_x/n-MgO-ME	$LiNO_3$	ME	25.0	21.8	63.1	13.8	37.9	23.8	35.6	2.7
LiC-TbO_x/n-MgO-ME	$LiCl_3$	ME	26.0	22.1	58.1	12.8	29.7	27.2	41.4	1.6
Li-TbO_x/n-MgO	$LiNO_3$	CIM	24.9	23.9	63.8	15.3	36.8	25.5	36.2	1.6
Li-TbO_x/n-MgO-SIM	$LiNO_3$	SIM	23.7	22.1	63.4	14.0	37.9	24.1	35.2	2.7
LiC-TbO_x/n-MgO	$LiCl_3$	CIM	23.8	22.0	57.5	12.6	28.8	27.8	41.5	1.9
LiC-TbO_x/n-MgO-SIM	$LiCl_3$	SIM	22.7	21.6	55.4	12.0	25.7	29.0	43.4	1.9

[a]REO loading is 20% by weight. Li loading is 2.5% by weight. [b]Preparation: IM = incipient wetness impregnation, ME = microemulsion, CIM = coimpregnated, SIM = sequential impregnation. [c]Overall methane conversion. Calculated as $(CH_{4in} - CH_{4out})/CH_{4in}$. [d]Methane conversion to CO_x and C_2 products only. [e]Percent of CH_4 converted to C_{2+} products. [f]Calculated as $X^*_{CH_4} \cdot S_{C_{2+}}$.

likely due to removal of Li from the catalyst surface, from the extended time-on-stream as well as the increasing temperature. It is interesting to note that the C_2H_4/C_2H_6 ratio is higher over the Li-doped compared with the undoped Sm_2O_3/n-MgO catalyst, and the ratio increases with increasing temperature (not shown). A higher C_2H_4/C_2H_6 ratio with increasing temperature is expected,[23] and addition of an alkaline-earth metal, such as Sr, to a Sm_2O_3 catalyst has been shown previously to increase this ratio.[38]

The behavior of the Li-TbO_x/n-MgO catalyst is different from both the Sm_2O_3-based catalysts. It has a more gradual light-off with increasing temperature than the Li-doped Sm_2O_3/n-MgO catalyst. The yield is similar to that obtained over the Sm_2O_3/n-MgO catalyst at 550 °C, despite the lower CH_4 conversion. Thus, the similar yield is due to a higher C_{2+} selectivity, and interestingly, the C_{2+} selectivity is higher over the Li-TbO_x/n-MgO catalyst than either of the Sm_2O_3-based catalysts at most of the temperatures investigated. Between 550 and 650 °C, the CH_4 conversion increases from 16% to 24%, and the C_{2+} selectivity, from 56% to 65%. Therefore, the maximum C_{2+} yield obtained over this catalyst is 14.9%, which is similar to that obtained over the Sm_2O_3/n-MgO catalyst, and it is obtained at a temperature as low as 650 °C. Compared with the Li-Sm_2O_3/n-MgO catalyst, the CO_2/CO ratio is significantly higher on the Li-TbO_x/n-MgO catalyst because of a lower CO concentration. Above 650 °C, there is a slight decline in the C_{2+} selectivity due to an increase in both CO and CO_2 product formation. A decrease in C_{2+} selectivity with temperature over Sr-doped Sm_2O_3 catalysts has been observed,[37] even though most OCM catalysts, such as Li/MgO[39] and the state-of-the-art Mn-Na_2WO_4/SiO_2 catalyst,[40] appears to yield an increase in C_{2+} selectivity with temperature. The decrease in C_{2+} selectivity with temperature is likely due to the rather low CH_4/O_2 ratio because at higher CH_4/O_2 ratios, REO catalysts are more likely to exhibit an increase in C_{2+} selectivity with temperature because the O_2 concentration is low and can limit the CO_x formation.[16,23,41] As expected, the C_2H_4/C_2H_6 ratio increases with temperature,[16] and at 650 °C and above, more C_2H_4 is formed than C_2H_6. Thus, although the maximum yield is obtained at 650 °C, the concentration of the more valuable C_2H_4 product increases with temperature, and the decrease in C_2 yield is not drastic between 650 and 800 °C. For example, the C_{2+} yield decreases from 14.9% to 12.6% between 650 and 800 °C, while the C_2H_4/C_2H_6 ratio increases from 1.1 to 2.5 in this temperature range.

3.1.2. Effects of Catalysts Preparation Method and Li Precursor. The effects of the catalyst preparation method and lithium precursor on the MgO-supported Sm_2O_3 and TbO_x catalysts were investigated at a reaction temperature of 700 °C. The activity, selectivity, and product distribution are presented in Table 1. The Sm_2O_3/n-MgO-ME catalyst (prepared using the microemulsion method) yields results very similar to those for the Sm_2O_3/n-MgO catalyst prepared using incipient wetness impregnation. The main differences between these two catalysts are a slightly lower C_2H_4/C_2H_6 ratio and somewhat higher CO_2/CO ratio for the Sm_2O_3/n-MgO-ME catalyst. The same trend in product ratios is observed over the TbO_x/n-MgO catalysts, but in this case, the TbO_x/n-MgO-ME catalyst is both more active and selective than the TbO_x/n-MgO catalyst prepared via IWI. However, the advantage with using the microemulsion technique to prepare TbO_x catalysts is diminished once lithium is added to the catalyst. There is not a significant difference in performance of the Li-Sm_2O_3/n-MgO and Li-Sm_2O_3/n-MgO-ME catalysts, either. Thus, the more cost-effective incipient wetness impregnation can be used to prepare these catalysts without any negative effects.

For the samaria catalysts, there is not a significant difference between catalysts prepared using different lithium precursors, regardless of preparation method used (Table 1). Furthermore, the preparation methods, microemulsion versus co- or sequential impregnation, do not have a significant effect on the activity and selectivity over the samaria catalysts. In contrast, the $LiNO_3$ precursor results in higher C_{2+} yields compared with the LiCl precursor for the Li-TbO_x/n-MgO catalysts. This result is independent of the preparation methods used in this study. The higher yield over the TbO_x/n-MgO

dx.doi.org/10.1021/cs500138j | ACS Catal. 2014, 4, 1972−1990

catalysts prepared using the $LiNO_3$ precursor is due to a higher selectivity compared with the catalysts prepared using the LiCl precursor.

Considering the results from the lithium precursor and preparation methods study, the $LiNO_3$ precursor and the simpler coimpregnation method were selected to prepare the undoped and Li-doped samaria and terbia catalysts for the time-on-stream study.

3.1.3. Time-On-Stream OCM Activity Measurements. Because Li-doped catalysts are known to deactivate with time on-stream, the catalytic activity and selectivity of the Sm_2O_3/n-MgO and TbO_x/n-MgO catalysts with and without lithium doping were evaluated at 650 and 700 °C for 8 h. These two temperatures were selected because the maximum C_{2+} yield was observed in this range for all the catalysts under investigation. Although the undoped TbO_x/n-MgO catalyst was not included in the temperature study, it was included in these measurements for comparison and also to determine the deactivation rate of a terbia catalyst without added lithium. The n-MgO support and two Li/n-MgO catalysts were included in this study to determine the effects of the support and the Li/MgO combination in these catalysts as well as to have a reference for the stability of the lithium containing catalysts. The results are presented in Tables 2 and 3 and Figures 2 and 3.

Table 2. Reaction Data for the Oxidative Coupling of Methane Obtained from MgO-Supported, Undoped and Li-Doped, Sm_2O_3 and TbO_x Catalysts after 8 h on-Stream

catalyst description[a]	rxn temp, °C	X_{CH_4}, %[b]	X_{CH_4}, %[c]	S_{C_2}, %[d]	Y_{C_2}, %[e]	Y_{C_2} loss, %[f]	SSA, m^2/g[g]
n-MgO[h]	650	22.1	17.8	39.8	7.1		20.4
	700	21.9	18.0	40.4	7.3		
Li(N)	650	3.6	2.4	47.4	1.1	5.4	2.1
	700	15.9	12.9	55.7	7.2	28.5	
Li(C)	650	5.1	3.6	55.6	2.0	17.4	3.0
	700	17.9	13.2	59.1	7.8	41.3	
Sm_2O_3	650	22.0	20.3	49.0	10.0	12.1	26.0
	700	22.4	20.3	49.9	10.1	13.0	
Li-Sm_2O_3	650	5.9	5.2	56.5	2.9	74.6	2.7
	700	22.7	19.6	57.3	11.2	24.4	
TbO_x	650	16.7	15.7	32.7	5.2	18.9	21.8
	700	18.9	17.3	38.0	6.6	9.8	
Li-TbO_x	650	21.9	20.0	62.1	12.5	16.9	5.9
	700	23.0	21.1	60.0	12.6	19.0	
	700[i]	22.2	18.8	50.2	9.5	29.6	

[a]All catalysts are supported on n-MgO, and REO loading is 20% by weight. Li loading is 2.5% by weight. [b]Overall methane conversion. Calculated as $(CH_{4in} - CH_{4out})/CH_{4in}$. [c]Gas phase CH_4 conversion to CO_x and C_2 products only. [d]Percent of CH_4 converted to C_2 products. [e]Calculated as $X^*_{CH_4} \cdot S_{C_2}$. [f]Percent loss of activity after 8 h on-stream. [g]SSA: specific surface area (m^2/g). [h]Initial reaction data point collected for n-MgO support only. [i]Reaction data after 30 h time on-stream.

3.1.3.1. n-MgO and Li/n-MgO Catalysts. The n-MgO support is surprisingly active at the reaction temperatures investigated (Table 2). A methane conversion of 22% is similar to the value obtained for pure Sm_2O_3 and only slightly lower than that obtained over the Sm_2O_3/n-MgO catalyst (24%), and although the C_{2+} selectivity (40%) is lower than that obtained over pure Sm_2O_3 (44%)[23] and Sm_2O_3/n-MgO (52%) (Table 1), it is higher than some reported values for doped MgO.[11] This suggests that the MgO nanoparticles contain impurities that are favorable in the OCM reaction because undoped MgO typically exhibits lower selectivities.[3] This may be due to trace amounts of sodium in the n-MgO because this and a trace amount of chlorine are the only impurities detectable in the XPS spectrum obtained from the pure nanoparticles (not shown).

Table 3. Product Distribution Obtained in the Oxidative Coupling of Methane over MgO-Supported, Undoped and Li-Doped, Sm_2O_3 and TbO_x Catalysts at the Beginning of the Experiment As Well As after 8 h On-Stream

		product distribution, %					
catalyst description[a]	rxn temp, °C	C_2H_4	C_2H_6	CO_2	CO	C_2H_4/C_2H_6 ratio	CO_2/CO ratio
n-MgO	650[b]	22.4	17.4	54.6	5.6	1.3	9.8
	700[b]	23.2	17.3	54.8	4.7	1.3	11.7
Li(N)	650[b]	7.3	37.9	45.9	8.9	0.2	5.2
	650[c]	7.5	39.9	44.0	8.6	0.2	5.1
	700[b]	37.3	19.7	32.2	10.8	1.9	3.0
	700[c]	34.8	20.5	28.4	16.4	1.7	1.7
Li(C)	650[b]	11.9	38.6	45.8	3.7	0.3	12.4
	650[c]	11.0	44.6	40.5	3.9	0.2	10.4
	700[b]	40.2	18.1	31.0	10.8	2.2	2.9
	700[c]	37.0	21.4	25.4	16.2	1.7	1.6
Sm_2O_3	650[b]	26.0	26.8	42.4	4.8	0.9	8.8
	650[c]	22.1	26.3	47.6	4.0	0.8	11.8
	700[b]	28.7	25.0	41.5	4.8	1.1	8.6
	700[c]	24.2	25.1	46.7	4.0	1.0	11.8
Li-Sm_2O_3	650[b]	35.9	25.6	33.0	5.5	1.4	6.0
	650[c]	18.9	37.5	36.8	6.8	0.5	5.4
	700[b]	38.1	22.7	36.0	3.2	1.7	11.3
	700[c]	37.2	19.1	33.5	10.3	1.9	3.2
TbO_x	650[b]	13.4	23.6	61.0	2.0	0.6	30.5
	650[c]	11.3	21.2	66.0	1.5	0.5	43.0
	700[b]	17.7	22.4	57.3	2.6	0.8	22.0
	700[c]	16.1	21.7	60.0	2.2	0.7	26.8
Li-TbO_x	650[b]	31.2	31.2	37.2	0.4	1.0	93.0
	650[c]	33.6	27.1	36.4	2.9	1.2	12.7
	700[b]	33.6	30.0	36.7	0.5	1.1	73.4
	700[c]	35.3	23.4	38.3	3.0	1.5	12.6
	700[d]	32.1	18.2	44.1	5.6	1.8	7.9

[a]All catalysts are supported on n-MgO, and REO loading is 20% by weight. Li loading is 2.5% by weight. [b]Initial reaction data point. [c]Reaction data after 8 h on-stream. [d]Results after 30 h on-stream.

Adding lithium to the magnesia support actually decreases the activity; the reference Li/n-MgO catalysts exhibit a lower methane conversion at 650 °C (Table 2). However, the C_{2+} selectivity is higher over the Li/n-MgO compared with the n-MgO support. The Li/n-MgO catalyst prepared using the carbonate precursor {Li(C)/n-MgO} performs better than the Li(N)/n-MgO catalyst in terms of both C_{2+} selectivity and CH_4 conversion. Both Li/n-MgO catalysts display some deactivation, but the activity is so low that it is difficult to comment on the severity of the activity loss (Figure 2).

At a reaction temperature of 700 °C, the activity and selectivity for both Li/n-MgO catalysts are significantly higher compared with the 650 °C results. The Li(C)/n-MgO catalyst exhibits the better initial performance of the two catalysts with a CH_4 conversion of almost 20% and a C_{2+} selectivity of 59.1%.

dx.doi.org/10.1021/cs500138j | ACS Catal. 2014, 4, 1972−1990

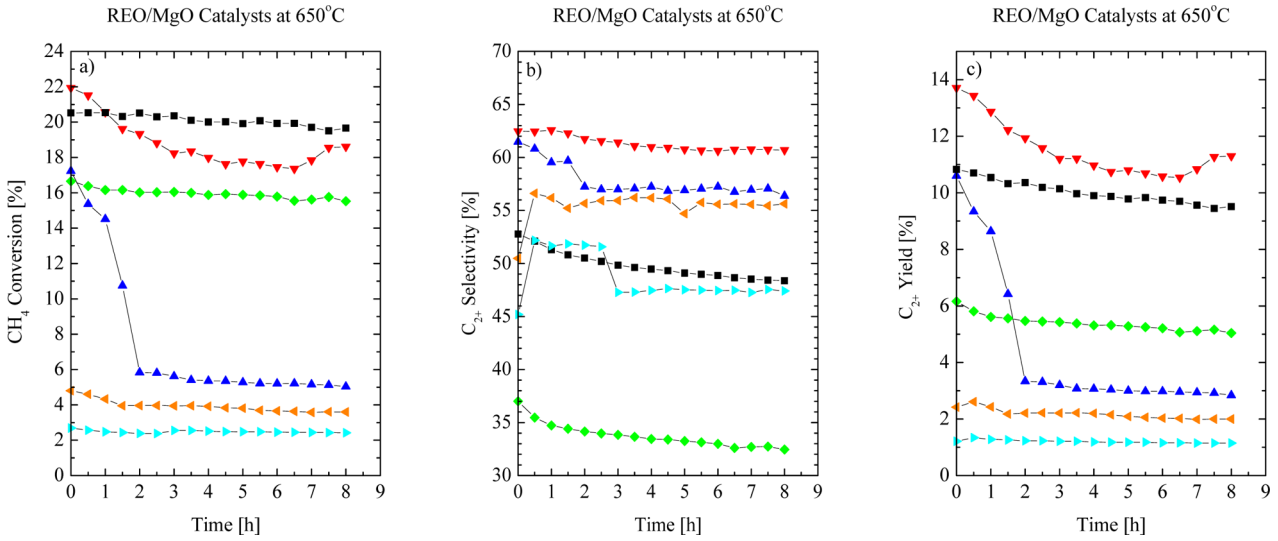

Figure 2. Oxidative coupling of methane reaction data stability experiments at 650 °C for different catalysts supported on n-MgO: (red ▼) Li-TbO_x, (dark blue ▲) Li-Sm_2O_3, (black ■) Sm_2O_3, (green ◆) TbO_x, (light blue right-pointing triangle) Li(N), (orange left-pointing triangle) Li(C).

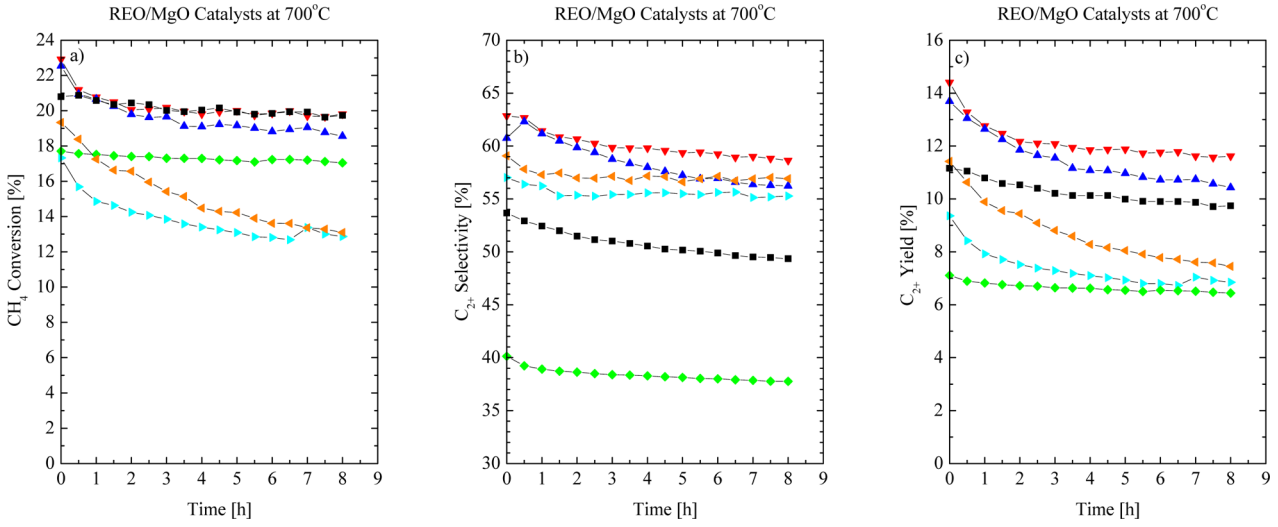

Figure 3. Oxidative coupling of methane reaction data for stability experiments at 700 °C for different catalyst systems supported on n-MgO: (red ▼) Li-TbO_x, (dark blue ▲) Li-Sm_2O_3, (black ■) Sm_2O_3, (green ◆) TbO_x, (light blue right-pointing triangle) Li(N), (orange left-pointing triangle) L(C).

However, compared with the Li(N)/n-MgO catalyst, the Li(C)/n-MgO catalyst experience a significantly higher drop in activity, and after 8 h on-stream, the CH_4 conversion is only 12.9%, which is similar to the 12.8% conversion obtained from the Li(N)/n-MgO catalyst. Although there is a small drop in C_{2+} selectivity during the first 2 h for both Li/n-MgO catalysts, the C_{2+} selectivity is fairly stable during the rest of the run. With time on-stream, slightly more CO is formed, while the CO_2 and the C_2H_4 concentrations are both lower compared with the initial product distribution (Table 3). Therefore, the activity loss (lower methane conversion) is the main reason for the lower C_{2+} yield after 8 h on-stream for these catalysts. The product distributions over the two Li/n-MgO catalysts are similar (Table 3) but depend strongly on the temperature. At a reaction temperature of 650 °C, the C_2H_4/C_2H_6 ratio is between 0.2 and 0.3, whereas at 700 °C, this ratio is between 1.7 and 2.2 for the Li/n-MgO catalysts. There is also a significant decrease in the CO_2/CO ratio when the temperature is increased from 650 to 700 °C. Although the C_2H_4/C_2H_6 ratio is not altered significantly, the CO_2/CO ratio decreases with time on-stream (Table 3).

In summary, the Li/n-MgO catalysts are not very active at 650 °C, but they do exhibit a reasonable initial activity and selectivity in the OCM reaction at 700 °C. However, as expected,[4] they are not very stable catalysts. The initially more active Li(C)/n-MgO catalyst exhibits a more severe deactivation and, thus, has an activity similar to the Li(N)/n-MgO catalyst after the 8 h on-stream. The main reason for the loss in yield over these catalysts with time on-stream is due to a lower methane conversion.

3.1.3.2. Sm_2O_3/n-MgO Catalysts. The Sm_2O_3/n-MgO catalyst yields very similar time-on-stream results at the two reaction temperatures (650 and 700 °C), with the C_{2+} yields after 8 h being 10.0% and 10.1%, respectively (Figures 2 and 3). This is in the range reported for pure Sm_2O_3 catalysts.[17] Compared with the Li/n-MgO catalysts, the CH_4 conversion is higher, but the C_{2+} selectivity is lower (or similar) over the Sm_2O_3/n-MgO catalyst. The initial C_{2+} yield obtained over the

dx.doi.org/10.1021/cs500138j | ACS Catal. 2014, 4, 1972−1990

Li(C)/n-MgO catalyst is slightly higher than that obtained over the Sm_2O_3/n-MgO catalyst; however, the Sm_2O_3/n-MgO catalyst is significantly more stable with time on-stream. At both temperatures, the Sm_2O_3/n-MgO catalyst exhibits only a slight decrease in C_{2+} yield with time on-stream, which is mainly due to a loss in the C_{2+}selectivity, although there is also a slight decrease in methane conversion over the 8 h experiment. Therefore, after 8 h on-stream, the Sm_2O_3/n-MgO catalyst is significantly more active than either of the Li/MgO catalysts. The C_2H_4/C_2H_6 ratio decreases with increasing time on-stream for the Sm_2O_3/n-MgO catalyst as a result of a decrease in the amount of C_2H_4 product because the C_2H_6 formation is uniform for the 8 h experiment. The CO_2 product formation increases with time on-stream while the CO formation is fairly constant. Thus, the loss in C_{2+} yield appears to occur from complete oxidation of C_2H_4 to CO_2 and H_2O. This trend is observed at both reaction temperatures (Table 3). Although the CO_2/CO ratio is roughly the same, there is a slight increase in the C_2H_4/C_2H_6 ratio between 650 and 700 °C, but the increase is not sufficient to warrant a higher reaction temperature. Therefore, because there is no benefit to increasing the temperature, it would be recommended to operate the Sm_2O_3/n-MgO catalyst at 650 °C instead of 700 °C.

The effects of adding lithium to the Sm_2O_3/n-MgO catalyst are dependent on the temperature of reaction. At 650 °C, doping with lithium increases the C_{2+} selectivity but decreases the CH_4 conversion compared with undoped Sm_2O_3/n-MgO catalyst. This effect has been observed previously.[26] The net result is that the initial C_{2+} yields are the same over the Sm_2O_3/n-MgO and Li-Sm_2O_3/n-MgO catalysts. However, after only a few hours on-stream, the CH_4 conversion has dropped from 17% to 5.8%, indicating that this is not a stable catalyst. There is also a drastic change in the C_2H_4/C_2H_6 ratio with time on-stream (Table 3). Initially, more C_2H_4 is formed, but after 8 h on-stream, significantly more C_2H_6 is formed than C_2H_4. At a reaction temperature of 700 °C, both the C_{2+} selectivity and CH_4 conversion are initially higher over the lithium-doped as compared with the undoped Sm_2O_3/n-MgO catalyst. However, compared with the Sm_2O_3/n-MgO catalyst, both the C_{2+} selectivity and CH_4 conversion exhibit a faster decline with time on-stream over the Li-Sm_2O_3/n-MgO catalyst. Nevertheless, the Li-Sm_2O_3/n-MgO catalyst is more stable at 700 °C than at 650 °C, which is consistent with observations for Li/MgO catalysts.[4] Although the initial C_{2+} yield is significantly higher over the Li-Sm_2O_3/n-MgO catalyst, after 8 h on-stream, the C_{2+} yield approaches that of the Sm_2O_3/n-MgO catalyst. The loss in C_{2+} yield is more significant for the Li-Sm_2O_3/n-MgO compared with the Sm_2O_3/n-MgO catalyst, but it is not as high as for the Li(C)/n-MgO catalyst. Furthermore, the major cause of the loss in C_{2+} yield is due to decreased C_{2+} selectivity (after 8 h on-stream, more CO_2 and less C_2H_4 is formed compared with the initial product distribution) over the Li-Sm_2O_3/n-MgO catalysts, rather a drop in CH_4 conversion as observed for the Li/n-MgO catalysts. The influence of Li doping on the product distribution at 700 °C is an increase in the C_2H_4/C_2H_6 ratio and decrease in the CO_2/CO ratio (less CO_2 and more CO is formed); therefore, the change in product distribution with time on-stream, a lower C_2H_4/C_2H_6 ratio and a higher CO_2/CO ratio, is consistent with loss of lithium.

3.1.3.3. TbO_x/n-MgO Catalysts. The lower C_{2+} yield obtained over the TbO_x/n-MgO catalyst compared with the Sm_2O_3/n-MgO is expected because terbia is a better oxidation catalyst than samaria. Nevertheless, the initial C_{2+} selectivity is reasonably high, between 30% and 40%, which is likely due to the n-MgO support, but it decreases with time on-stream. Both the C_2 products C_2H_4 and C_2H_6 decrease, while the contribution from CO_2 in the product stream is higher after 8 h on-stream. In addition to the lower C_{2+} selectivity, the CH_4 conversion is also slightly lower than the conversions obtained from the n-MgO support and the Sm_2O_3/n-MgO catalyst (Table 2). Because the activity is so low for the Li/MgO catalysts, the C_{2+} yield at 650 °C is higher over the TbO_x/n-MgO catalyst despite the low C_{2+} selectivity. At 700 °C, the C_{2+} yield is higher than at 650 °C, but it is now lower than the C_{2+} yields obtained over the Li/MgO catalysts, at least initially. Because the TbO_x/n-MgO catalyst is more stable than the Li/MgO catalysts, the difference in C_{2+} yields between these catalysts is only 1% after 8 h on-stream.

Adding lithium to the TbO_x/n-MgO catalyst increases both the CH_4 conversion and the C_{2+} selectivity. In fact, at 650 °C, the increase in the C_{2+} yield is over 100% when lithium is added to the MgO-supported TbO_x catalyst. The majority of the improvement is from the enhanced C_{2+} selectivity, which nearly doubles with the addition of lithium (32.7% for undoped and 62.1% for Li-doped TbO_x/n-MgO). This is a very high value for a TbO_x catalyst, and it is a high selectivity also for other OCM catalysts at a CH_4/O_2 ratio as low as 4.[23] Furthermore, the Li-TbO_x/n-MgO catalyst is significantly more stable than the Li-Sm_2O_3/n-MgO catalyst, particularly at 650 °C. The deactivation rate for this catalyst appears to be similar to that of the undoped TbO_x/n-MgO catalyst. As for the Sm_2O_3-based catalysts, the activity loss is mainly due to a drop in C_{2+} selectivity with time on-stream over the TbO_x/n-MgO catalyst, as opposed to the drop in CH_4 conversion observed over the Li/MgO catalysts. The effects of Li doping on the product distribution of TbO_x/n-MgO catalysts is similar to the effects of adding Li to Sm_2O_3/n-MgO catalyst (at 700 °C), that is, the C_2H_4/C_2H_6 ratio increases, and the CO_2/CO ratio decreases. In fact, even at 650 °C, the Li-TbO_x/n-MgO catalyst achieves a C_2H_4/C_2H_6 ratio >1.0, which is remarkable because the most active Sm_2O_3/Al_2O_3 catalyst required 800 °C to do so.[25] If deactivation was due solely to Li leaving the catalyst, it may be expected that the C_2H_4/C_2H_6 ratio will decrease with time on-stream. In contrast, the C_2H_4/C_2H_6 ratio increases with time on-stream over the Li-TbO_x/n-MgO catalyst, which means that more of the formed C_2H_6 is converted to C_2H_4. The concentration of both CO and CO_2 is also increased with time on-stream. This may suggest that the contribution from surface reaction increases with time on-stream, compared with the gas phase radical reaction to form C_2H_6; however, there is not a significant change in the surface area of this catalyst with time on-stream.

Previous studies using a lithium-doped magnesium oxide catalyst[4] found that the severity of catalyst deactivation was strongly correlated with the initial loading of lithium on the catalyst. Loadings of 2% and above underwent severe deactivation within the first few hours of exposure to OCM reaction conditions and, depending on the preparation method for the Li containing catalyst, could reach as high as 70% loss of activity. The optimum lithium doping in the study was found to be 0.5%, although even at this Li loading, the deactivation was significant. Our Li-REO/n-MgO catalysts deactivate at a much slower rate than both the Li/MgO catalysts studied by Arndt and the two reference systems prepared in our lab. Particularly interesting is the behavior by the Li-TbO_x/n-MgO catalysts at

dx.doi.org/10.1021/cs500138j | ACS Catal. 2014, 4, 1972−1990

650 °C compared with the undoped TbO_x/n-MgO sample. After 8 h of time on-stream, the activity loss for the two catalysts is 18.9% and 16.9%, respectively. However, at 700 °C, the deactivation for the lithium-doped sample is greater than the undoped terbia catalyst. This is in contrast to the Li/MgO systems reported in the literature, for which the higher reaction temperatures resulted in more stable catalysts.[4]

3.1.4. Long-Term Stability Test of Li-TbO_x/n-MgO. A long-term stability test was performed at a reaction temperature of 700 °C on the most active and stable catalyst, the Li-TbO_x/n-MgO, to investigate the behavior at longer times on-stream. The reaction results (CH_4 conversion, C_{2+} selectivity, and C_{2+} yield) are presented in Figure 4 and have been added to Tables

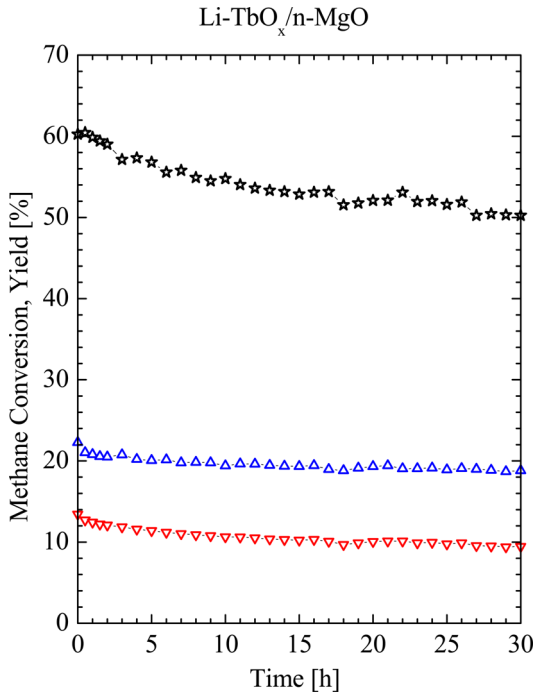

Figure 4. Oxidative coupling of methane reaction results for long-term stability testing of Li−TbO_x/n-MgO at 700 °C: (blue △) methane conversion to gas phase products, (☆) C_{2+} selectivity, (red ▽) C_{2+} yield.

2 and 3. Despite the promising results of the 8 h experiment, this catalyst continues to deactivate at a low but fairly constant rate during the 30 h on-stream. The 30% loss in C_{2+} yield after 30 h on-stream (initial yield of 13.5% and final yield of 9.5%) is due to a small drop in CH_4 conversion (from 22% to 18.5%) as well as a more significant loss in C_{2+} selectivity (from 60% to 50%). Of course, this 30% loss in C_{2+} yield after 30 h is to be compared with the 40% loss in C_{2+} yield over the Li(C)/n-MgO catalyst after only 8 h on-stream. The C_2H_6 product flow rate decreases over twice as much as the C_2H_4 flow rate (20% for C_2H_4 compared to 42% for C_2H_6). These results suggest that the activity loss is due to a lower methyl hydrogen abstraction rate with time on-stream, that is, the catalyst is losing active sites. However, as more of the C_2H_6 product is dehydrogenated to C_2H_4, the dehydrogenation sites do not seem to be affected to the same extent. In addition, the surface sites that generate CO and CO_2 appear to increase. Because the C_{2+} yield never reaches a steady-state value during the long-term reaction study, it must be assumed that this catalyst would continue to lose activity, and that, even though it is more stable than the Li/n-MgO catalyst, finding an alternative promoter is highly desirable.

3.2. Catalyst Characterization. The magnesia-supported REO catalysts with and without lithium doping, as well as the nanoparticle magnesia support, were subjected to catalyst characterizations to determine properties of importance for the catalytic activities and selectivities and determine the effects on the catalyst during the time on-stream experiments. The results from each technique are presented below.

3.2.1. BET Surface Area Measurements. The BET surface area of the undoped and lithium-doped REO supported on magnesia catalysts after calcinations at 800 °C are presented in Table 2. The surface area of the nanoparticle MgO support (20.4 m^2/g after calcination at 800 °C) was also measured and included for reference. The as-prepared TbO_x/n-MgO and Sm_2O_3/n-MgO catalysts have surface areas of 21.8 and 26.0 m^2/g, respectively. Thus, adding the REOs to the n-MgO support results in a slight increase in the overall surface area versus the bare support surface area. In contrast, the surface areas of the as-prepared Li-doped TbO_x/n-MgO and Sm_2O_3/n-MgO catalysts are almost an order of magnitude smaller than the undoped catalysts at only 5.9 and 2.7 m^2/g, respectively. A lower surface area after addition of lithium has been observed previously[2] and is consistent with the surface areas of the two Li/MgO reference systems, 2.1 and 3.0 m^2/g for the Li(N)/n-MgO and Li(C)/n-MgO, respectively. The BET data reveal that there is no simple correlation between the overall catalyst surface area and the activity or selectivity for these catalysts. Once there is sufficient active surface area to activate methane toward hydrogen abstraction, increasing the surface area of the catalyst can decrease the selectivity and may therefore result in a lower product yield. Thus, even though the surface areas are rather low for a catalyst, this indicates that the surface area is not the limiting factor for these catalysts under the conditions used in the study.

3.2.2. XRD Analysis. The XRD patterns of the fresh Li-doped and undoped TbO_x/n-MgO and Sm_2O_3/n-MgO are shown in Figures 5 and 6. The XRD pattern of the pure n-MgO support after calcinations at 800 °C for 4 h was also collected (not displayed) to make sure that the particle size of the support is not significantly altered by deposition of the rare earth oxides. Table 4 reveals that the MgO particle size on the

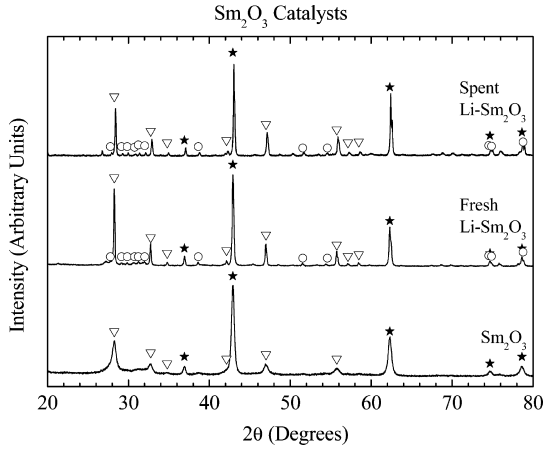

Figure 5. XRD data obtained from fresh undoped, Li-doped, and spent Li-doped Sm_2O_3/n-MgO. The labels indicate the following crystal phases: ▽, Sm_2O_3(cubic); ○, Sm2O3 (monoclinic); ★, MgO.

dx.doi.org/10.1021/cs500138j | ACS Catal. 2014, 4, 1972−1990

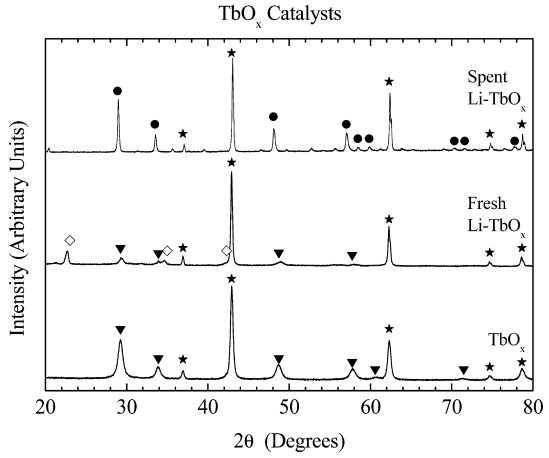

Figure 6. XRD data obtained from fresh undoped, Li-doped, and spent Li-doped TbO_x/n-MgO catalysts. The labels indicate the following crystal phases: ▼, TbO_x; ◊, Li_2CO_3; ●, Tb_2O_3; and ★, MgO.

Table 4. Particle Size Calculations Using the Scherrer Equation and XRD Data Obtained from Selected Catalysts

	particle size [nm]		
catalyst	Sm_2O_3[a]	TbO_x	MgO
n-MgO[b]			20.0
Sm_2O_3/n-MgO[b]	11.4		21.3
Li-Sm_2O_3/n-MgO[b]	54.6		37.1
Li-Sm_2O_3/n-MgO spent[c]	48.2		42.7
TbO_x/n-MgO[b]		11.9	23.7
Li-TbO_x/n-MgO[b]		16[d]	34.8
Li-TbO_x/n-MgO spent[c]		39.1	40.7

[a]Cubic phase of Sm_2O_3. The peaks due to monoclinic Sm_2O_3 were too small for particle size determination. [b]After calcination at 800 °C. [c]After 8 h on-stream. [d]The signal-to-noise ratio for the TbO_x crystalline peaks for this sample was very low, so the accuracy of the calculation is lower compared with the other peaks.

bare support and the undoped TbO_x/n-MgO and Sm_2O_3/n-MgO are very similar. The main phases present in the fresh Sm_2O_3/n-MgO catalyst are cubic Sm_2O_3 and cubic MgO with no major impurities. In contrast, the coprecipitation of lithium and samaria results in a monoclinic form of Sm_2O_3 in addition to the cubic Sm_2O_3 phase on the n-MgO support (Figure 5). No lithium-containing compounds were detected in the XRD analysis, which means that the added lithium does not form large crystalline particles of lithium-containing phases under these conditions. However, it does not rule out formation of amorphous or small segregated lithium compounds on the surface because they would be XRD-invisible. Particle size calculations using the Scherrer equation reveal that both the cubic Sm_2O_3 and MgO crystallites are larger on the Li-doped versus undoped Sm_2O_3/n-MgO (Table 4). This is consistent with the lower BET surface area of the Li-doped catalyst.

The XRD pattern obtained from the fresh TbO_x/n-MgO suggests that the crystalline phase present is a slightly reduced TbO_2 phase, that is, a $TbO_{2-\delta}$ phase where $0 \leq \delta \leq 0.25$. Several reference XRD patterns from the literature for different terbia samples, particularly TbO_2, Tb_4O_7, and a $TbO_{1.81}$, were compared to assist in the assignment of the TbO_x phase. The reference data that fit most closely the peaks in the XRD pattern obtained from the TbO_x/n-MgO are assigned to a $TbO_{1.81}$ phase. However, the match is not exact, which leads us to refer to the phase as TbO_x, where $1.75 \leq x \leq 2$. The XRD pattern obtained from the fresh Li-TbO_x/n-MgO catalyst has two peaks in addition to the ones originating from the TbO_x and MgO phases. These two peaks are reasonably consistent with reference peaks from hexagonal Li_2CO_3, according to the database [JCPDS 072−6635], although other Li-containing phases cannot be excluded. Compared with the reference hexagonal Li_2CO_3 peaks, the peaks in the XRD pattern obtained from the fresh Li-TbO_x/n-MgO catalyst are shifted to slightly higher 2θ values, indicating that the hexagonal Li_2CO_3 lattice is distorted in the catalyst, and this could be due to interactions with the TbO_x on the surface.

The presence of Li-related peaks in the XRD pattern is different from the behavior of the Sm_2O_3/n-MgO catalyst, in which no peaks due to Li-based compounds could be detected using XRD. The peaks due to the $TbO_{1.81}$ phase obtained from the Li-TbO_x/n-MgO are smaller compared with the TbO_x/n-MgO catalyst, whereas the particle size according to the Scherrer equation is slightly larger (Table 4). This may be due to a lower crystallinity of the Li-TbO_x/n-MgO catalyst compared with the TbO_x/n-MgO. This behavior is also different from that of the undoped and Li-doped Sm_2O_3/n-MgO catalysts and suggests that the interactions between Li and TbO_x are different from the interactions between Li and Sm_2O_3. As for the Sm_2O_3-based catalysts, the MgO particles on the Li-TbO_x/n-MgO catalyst are larger than on the undoped TbO_x/n-MgO catalyst (Table 4). This indicates that the lithium is not incorporated into the bulk phase of MgO, although this has been observed under certain conditions.[42,43]

The monoclinic and cubic Sm_2O_3 mixture remains after exposure to reaction conditions at 700 °C for 8 h, which suggests that either an amount of lithium sufficient to stabilize the monoclinic Sm_2O_3 remains on the surface or the lithium-induced formation of monoclinic Sm_2O_3 is irreversible (Figure 6). Particle growth of the MgO is apparent in the XRD pattern obtained from the spent Li-Sm_2O_3/n-MgO catalyst: the peaks are significantly narrower compared with the fresh catalyst, and this is further supported by particle size calculations shown in Table 4. The crystallite size of cubic Sm_2O_3, however, appears to decrease slightly (from 54.6 to 48.1 nm) while the crystallite size of the monoclinic Sm_2O_3 is increased, as is evident in Figure 5. This indicates that some cubic Sm_2O_3 has been converted to the monoclinic phase, which is expected because prolonged exposure to temperatures as high as 800 °C may induce phase transformation to the monoclinic phase, which is the stable phase at higher temperatures.[44] The increase in monoclinic Sm_2O_3 after time on-stream may explain some of the catalyst deactivation, because the monoclinic Sm_2O_3 phase is less active and selective than the cubic Sm_2O_3 phase.[26] In addition, some particle growth is expected after prolonged exposure to high temperatures, which will reduce the Sm_2O_3 surface area available for reaction.

The Li-containing phase is no longer present in the XRD pattern obtained from the spent Li-TbO_x/n-MgO catalyst, which may be indicative of lithium leaving the surface of the catalyst during reaction. The TbO_x-related peaks are significantly more intense on the spent catalyst compared with the fresh, which reveals substantial particle growth. The TbO_x particle sizes increase from an average of 16 to 39 nm (Table 4). The peaks are also shifted from the original $TbO_{1.81}$ phase identified on the fresh Li-TbO_x/n-MgO catalyst. The peaks in the XRD pattern obtained from the spent Li-TbO_x/n-MgO catalyst are more consistent with the sesquioxide Tb_2O_3 phase

dx.doi.org/10.1021/cs500138j | ACS Catal. 2014, 4, 1972−1990

[JCPDS 76−156], which would mean that the $TbO_{1.81}$ was reduced during reaction. Despite removal of the Li-containing phase, which was present on the fresh catalyst, the Li-TbO_x/n-MgO catalyst is more stable than the other Li-doped catalysts in the study. The deactivation rate of this catalyst is similar to the undoped Sm_2O_3/n-MgO catalyst. This could indicate that deactivation due to loss of active surface area from sintering (particle growth) is an important deactivation pathway, in addition to Li-removal, over the Li-TbO_x/n-MgO catalysts.

3.2.3. TEM Analysis. Selected representative TEM images for lithium-doped and undoped Sm_2O_3/n-MgO and TbO_x/n-MgO catalysts after calcination at 800 °C for 4 h are presented in Figure 7. The Sm_2O_3/n-MgO and TbO_x/n-MgO catalysts consist of particles with average particle sizes between 20 and 50 nm. This is reasonably consistent with the particle sizes calculated using line-broadening of the XRD peaks. In addition, the particles in the Sm_2O_3/n-MgO catalyst appear to be slightly smaller than the particles of the TbO_x/n-MgO catalyst, which is consistent with the higher surface area of the Sm_2O_3/n-MgO catalyst. After doping with lithium there is a dramatic increase in the particle size of the catalyst, consistent with the decrease in BET surface area. The trend is also consistent with the increase in particle size determined from the XRD data, but the magnitude of the change is not captured with XRD. TEM indicates that the particles are larger than what is determined from XRD, which suggests that each particle in TEM consists of more than one crystallite. The particles appear to be more agglomerated in the Li-TbO_x/n-MgO catalyst, which could explain the significant reduction in surface area of this catalyst compared with the bare support or the undoped TbO_x/n-MgO catalyst. EDX was performed on the Li-REO/n-MgO catalysts in an attempt to identify lithium on the surface, but the attempts were unsuccessful because the atomic similarities between magnesium and lithium complicates the process.

3.3.4. XPS Measurements. The XPS data obtained from the fresh Li-doped and undoped Sm_2O_3/n-MgO and TbO_x/n-MgO catalysts are presented in Figures 8 and 9. The composition analysis from these narrow scans has been included in Table 5. The Mg 2p peaks due to the MgO support reveal that the electronic structure of the support is not significantly affected by the addition of rare earth oxide or lithium (Figure 8 a). The presence of lithium on the surface of the Li-Sm_2O_3/n-MgO and Li-TbO_x/n-MgO catalysts is evident as small peaks at a binding energy of 54.5 eV. The slightly higher peak intensity of the Li 1s peak in the spectrum obtained from the Li-Sm_2O_3/n-MgO catalyst indicates that the near-surface concentration of lithium is higher on this catalyst compared with the Li-TbO_x/n-MgO catalyst. This is also seen in the compositional analysis (Table 5) and appears to be due to terbia covering the lithium (the Tb $3d_{5/2}$ signal intensity is slightly higher on the Li-doped catalysts). For the Sm_2O_3-based catalysts, the addition of lithium reduces the intensity of the Sm $3d_{5/2}$ peak (revealing a lower surface concentration compared to the undoped catalyst; Table 5), which suggests that the lithium is covering some of the samaria on this catalyst surface. The magnesium concentration is also slightly lower, which could be due to some coverage by lithium species. There is no apparent shift in the Sm $3d_{5/2}$ peak for the lithium-containing catalyst (Figure 8 b), suggesting the lithium does not have a charge effect on the samaria on the surface. In contrast, lithium addition to the TbO_x/n-MgO results in a one-eV shift in the Tb $3d_{5/2}$ peak to higher binding energies (Figure 8 c). This is an indication of strong interactions between lithium and terbia and could explain the differences in behavior between the Sm_2O_3/n-MgO and TbO_x/n-MgO catalysts. It is possible that a small amount of the added Li enters the TbO_x lattice and forms an amorphous (and XRD-invisible) mixed Li-TbO_y phase. This would explain the lower intensities of the TbO_x peaks in the XRD pattern and the shift to higher binding energies of the Tb $3d_{5/2}$ peaks after Li doping as well as the lower intensity of the Li 1s peak in the XPS spectra obtained from the Li-TbO_x/n-MgO compared with the Li-Sm_2O_3/n-MgO.

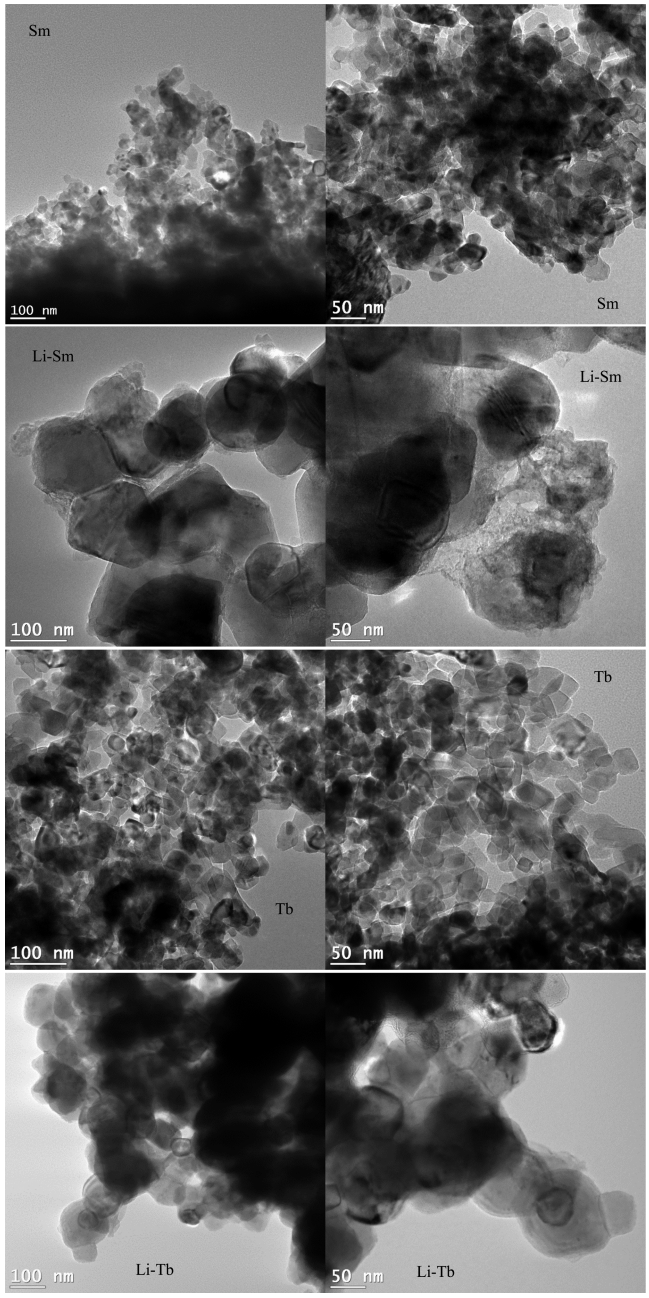

Figure 7. TEM images of undoped and lithium-doped REO/n-MgO catalysts at two different magnifications: Sm, Sm_2O_3/n-MgO; Li-Sm, Li-Sm_2O_3/n-MgO; Tb, TbO_x/n-MgO; and Li-Tb, Li-TbO_x/n-MgO. Left: low magnification; scale-bar, 100 nm. Right: high resolution; scale bar, 50 nm.

The O 1s and C 1s peaks obtained from the undoped and lithium-doped REO-supported catalysts also contain valuable information regarding these catalysts. Because some of O 1s

dx.doi.org/10.1021/cs500138j | ACS Catal. 2014, 4, 1972−1990

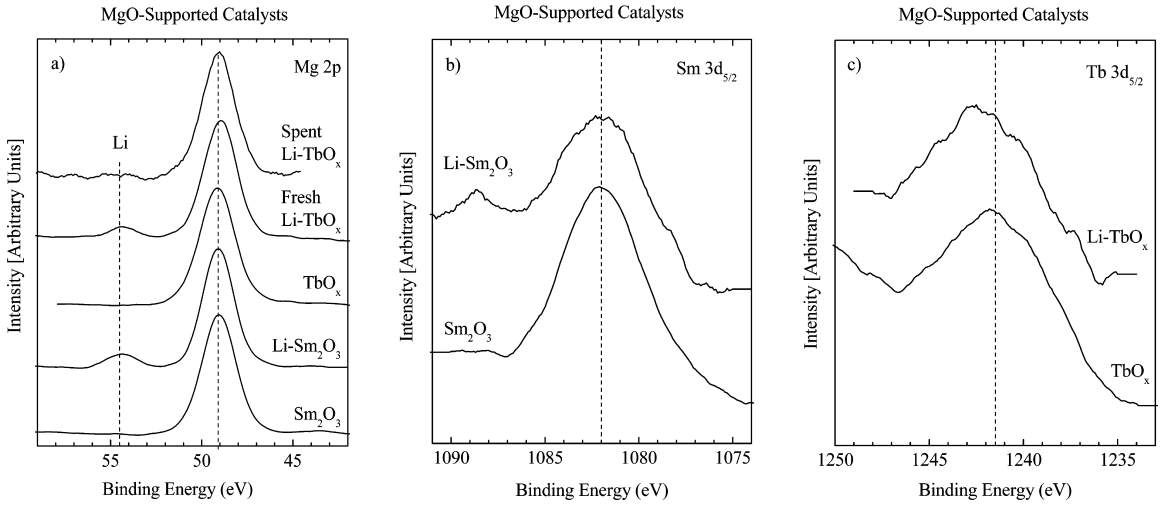

Figure 8. Narrow-scan XPS spectra of the (a) Li 1s and Mg 2p, (b) Sm $3d_{5/2}$, and (c) Tb $3d_{5/2}$ binding energy regions obtained from undoped and lithium-doped REO/n-MgO catalysts.

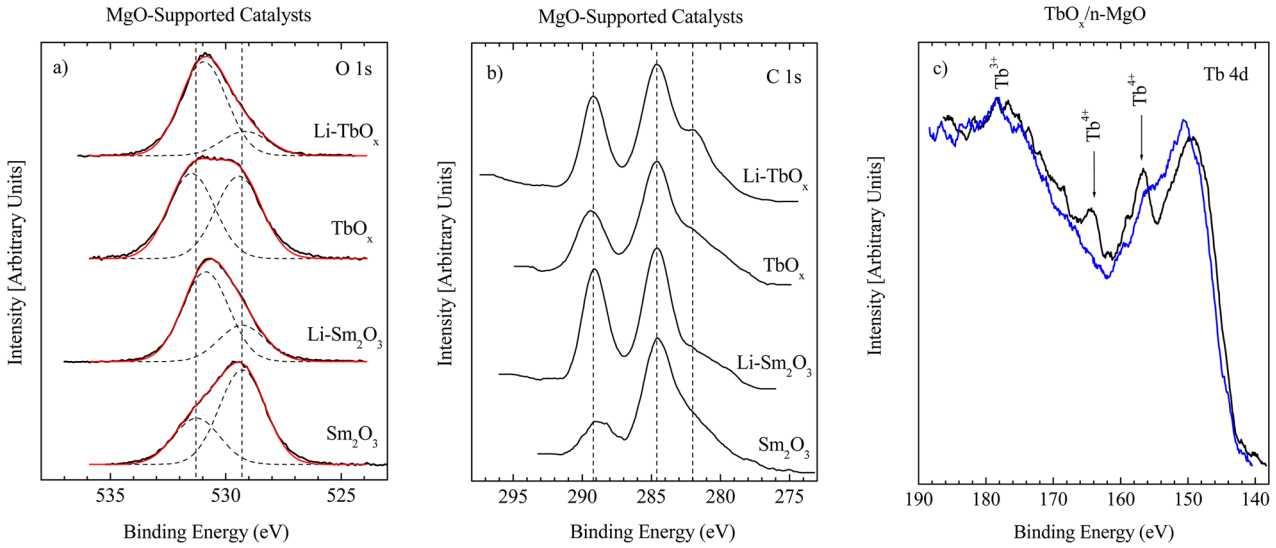

Figure 9. Narrow-scan XPS spectra of the (a) O 1s where the red trace is the Gaussian peak fit of the collected data and (b) C 1s binding energy regions obtained from fresh undoped and lithium doped REO/n-MgO catalysts, and (c) Tb 4d peaks obtained from fresh (black) and spent (blue) Li-TbO$_x$/n-MgO catalysts.

Table 5. XPS Compositional Analysis of Selected Catalysts

catalyst[a]	O 1s, %	Tb $3d_{5/2}$, %	Sm $3d_{5/2}$, %	Mg 2p, %	Li 1s, %	REO/Mg ratio	O/(REO+Mg) ratio	Li/REO ratio	$O^{II}/O^{I,b}$
Sm_2O_3/n-MgO	56		8	36		0.22	1.27		0.49
Li-Sm_2O_3/n-MgO	68		2	21	9	0.10	3.09	4.5	2.48
TbO$_x$/n-MgO	64	5		31		0.16	1.78		1.04
Li-TbO$_x$/n-MgO	65	6		23	6	0.26	2.24	1	3.86

[a]The following atomic sensitivity factors were used in the calculation of the compositions: O 1s, 0.711; Sm $3d_{5/2}$ = 2.907; Tb $3d_{5/2}$ = 3; Mg 2p = 0.12; Li 1s = 0.025.[36] [b]Peak area ratios of O 1s peaks from the peak fitting (for details, please see the Experimental section). The O^I is the O 1s peak between 529.1 and 529.5 eV, which is due to the MgO support and the rare earth oxides. The O^{II} peak located between 530.9 and 531.5 eV is due to hydroxyl groups and carbonates.

contribution is from carbonates (CO_2 adsorbed on the surface of these catalysts), it is useful to look at the O 1s and C 1s peaks together (Figure 9a,b). The binding energy of the main O 1s peak obtained from the Sm_2O_3/n-MgO catalyst is 529.3 eV, consistent with the values reported for MgO and Sm_2O_3;[36−45] however, a significant shoulder is present at binding energies between 530.9 and 531.5 eV, revealing the presence of surface hydroxyl and carbonate groups. The small C 1s peak at 289.0 eV confirms the presence of surface carbonates.

Addition of lithium to the Sm_2O_3/n-MgO catalyst increases the contribution from the state with an O 1s binding energy of 531.0 eV. The peak fitting to deconvolute the contributions from the metal oxides (MgO and Sm_2O_3 oxygen species labeled O^I) and the carbonates plus potential hydroxyl groups (oxygen species labeled O^{II}) is shown in Figure 9 and reveals that the

dx.doi.org/10.1021/cs500138j | ACS Catal. 2014, 4, 1972−1990

O^{II}/O^{I} ratio increases from 0.5 to 2.5 with the addition of lithium (Table 5). The main contribution to the O^{II} species after addition of lithium is due to carbonates, as evident in the high C 1s peak intensity at a binding energy of 289.2 eV. Because CO_2 is an acidic molecule that adsorbs onto basic sites, adsorption of CO_2 on the surface of these catalysts indicates the presence of basic sites. This is important because it is believed that basic oxygen sites are responsible for the hydrogen removal from methane, the first step in the oxidative coupling of methane.[3] Because Li_2CO_3 was observed in the XRD pattern obtained from the Li-TbOx/n-MgO catalyst, it is possible that Li_2CO_3 is also present on the surface of the Li-Sm_2O_3/n-MgO catalyst. However, in the case of the Li-Sm_2O_3/n-MgO catalyst, the surface amount appears to be too small for detection with XRD, or the Li_2CO_3 on this catalyst is amorphous.

The O 1s peak obtained from the TbO_x/n-MgO catalyst has a higher contribution from the state at 531.0 eV (O^{II}/O^{I} ratio of 1.0) compared with the undoped Sm_2O_3/n-MgO catalyst (O^{II}/O^{I} ratio of 0.5). This is due to a higher contribution from adsorbed carbonates on the TbO_x/n-MgO catalyst (versus the Sm_2O_3/n-MgO) as evident in the C 1s spectra. Similar to the Sm_2O_3-based catalysts, addition of lithium significantly increases the contribution from the 531.0 eV state (Figure 9a). The O^{II}/O^{I} ratio increases by a factor of 4 after lithium addition, and the majority of this increase is due to carbon dioxide adsorption, as is evident in the higher intensity of the 289.2 eV C 1s carbonate peak.

The lithium peak intensity is very close to the noise level in the spectrum obtained from the spent Li-TbO_x/n-MgO catalyst (Figure 8a). This is consistent with the XRD data, which revealed removal of the lithium-containing compound. Even though most of the Li appears to have been removed after reaction, the Li-doped TbO_x/n-MgO catalyst still has a significantly higher C_{2+} selectivity compared with the undoped catalyst, which suggests that either some residual lithium is still on the surface, or the positive effects of lithium are present even after the lithium has been removed. The Tb 4d peaks obtained from the spent Li-TbO_x/n-MgO catalyst reveal that the original $TbO_{1.81}$ phase is at least partially reduced (Figure 9 c). The intensities of the Tb^{4+}-related peaks are lower after reaction, which is consistent with the formation of a Tb_2O_3 phase as observed with XRD after reaction. Thus, the XPS data indicate that more CO_2 is adsorbed on the TbO_x/n-MgO catalyst (O^{II}/O^{I} ratio of 1.0) compared with the Sm_2O_3/n-MgO catalyst (O^{II}/O^{I} ratio of 0.5), and the amount of CO_2 adsorbed is increased on both catalysts after doping with lithium, as revealed by the O^{II}/O^{I} ratios for the two lithium-doped samples (2.5 for Li-Sm_2O_3/n-MgO and 3.9 for Li-TbO_x/n-MgO). Again, the higher contribution of adsorbed CO_2 is due in part to the presence of Li_2CO_3 on the surface of the catalyst. A larger contribution from the XPS peaks due to adsorbed CO_2 indicates a higher number of basic sites and indicates that the Li-TbO_x/n-MgO is the most basic catalyst of the ones included in this study. In addition, the TbO_x/n-MgO catalyst has a higher number of basic sites compared with the Sm_2O_3/n-MgO catalyst. This is somewhat unexpected because basic sites have been shown to be important in the OCM reaction.[26] If only the number of basic sites were important, it would be expected that the Sm_2O_3-based catalyst would have more adsorbed CO_2 because Sm_2O_3 catalysts are more active than TbO_x-based catalysts. Clearly, the character of the basic site, which would affect the strength of CO_2 adsorption, is very important in this reaction.

3.3.5. Temperature-Programmed Desorption of CO_2. Because a significant amount of CO_2 was observed with XPS on the fresh doped and undoped REO/n-MgO catalysts, the temperature-programmed desorption (TPD) of CO_2 from the TbO_x/n-MgO catalysts was investigated to determine the strength of CO_2 adsorption on these catalysts. TPD was carried out after a CO_2 dosing at 200 °C because CO_2 dosing at 50 °C did not yield sufficient chemisorption which was apparent by poor signal-to-noise. Thus, it appears that the CO_2 adsorption is activated and requires a minimum temperature. A temperature of 200 °C was chosen to ensure CO_2 adsorption on the surface while limiting CO_2 desorption from the most weakly bound sites before the TPD experiments. The n-MgO has a small amount of basic sites, but most of them are weakly basic. At a temperature of 600 °C, most of the CO_2 has been removed from the surface (Figure 10). The CO_2 adsorption on the

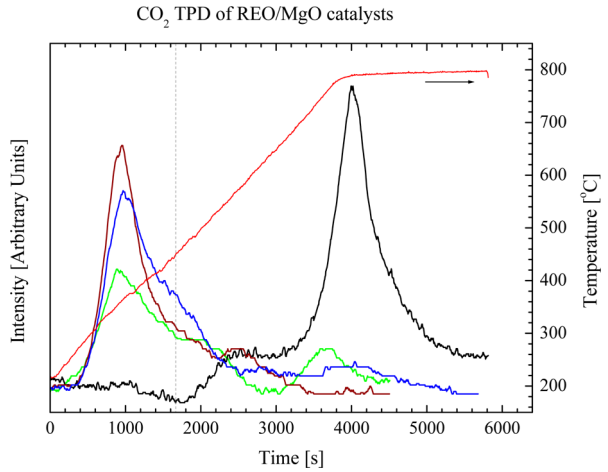

Figure 10. CO_2 TPD data obtained from the n-MgO support and selected n-MgO-supported catalysts after CO_2 dosing at 200 °C for 30 min. The red line indicates the temperature ramp; green, n-MgO support; brown, Sm_2O_3/n-MgO; blue, TbO_x/n-MgO; and black, Li-TbO_x/n-MgO.

Sm_2O_3/n-MgO and TbO_x/n-MgO catalysts is higher than on the n-MgO support; however, the adsorbed CO_2 is completely desorbed also on these catalysts by 500–600 °C (Figure 10). Thus, the strength of CO_2 adsorption is similar on the n-MgO support and the REO/n-MgO catalysts, but more CO_2 is adsorbed in the presence of the REOs. In stark contrast, very little CO_2 is desorbed from the Li-TbO_x/n-MgO catalyst before the temperature reaches 700 °C. The adsorption strength of CO_2 on the Li-TbO_x/n-MgO catalyst is clearly much higher, and the amount of CO_2 adsorbed is also higher than on the TbO_x/n-MgO catalyst. This is consistent with the XPS data, and on the basis of these data, the same trend is expected for the Sm_2O_3/n-MgO catalysts; that is, that the Li doping increases the amount and the strength of CO_2 adsorption. However, because of the volatility of lithium, which was clearly observed as deposits on the instrument after the analysis of the Li-TbO_x/n-MgO catalyst, it was decided not to run the Li-Sm_2O_3/n-MgO or Li/n-MgO catalysts to protect the equipment, and instead, it was decided to investigate the catalysts using DRIFTS.

3.3.6. DRIFTS Experiments. To probe the nature of the surface sites on the catalysts in this study (mainly the surface oxygen), in situ DRIFTS experiments after CO_2 adsorption at two different temperatures were performed on the fresh

dx.doi.org/10.1021/cs500138j | ACS Catal. 2014, 4, 1972–1990

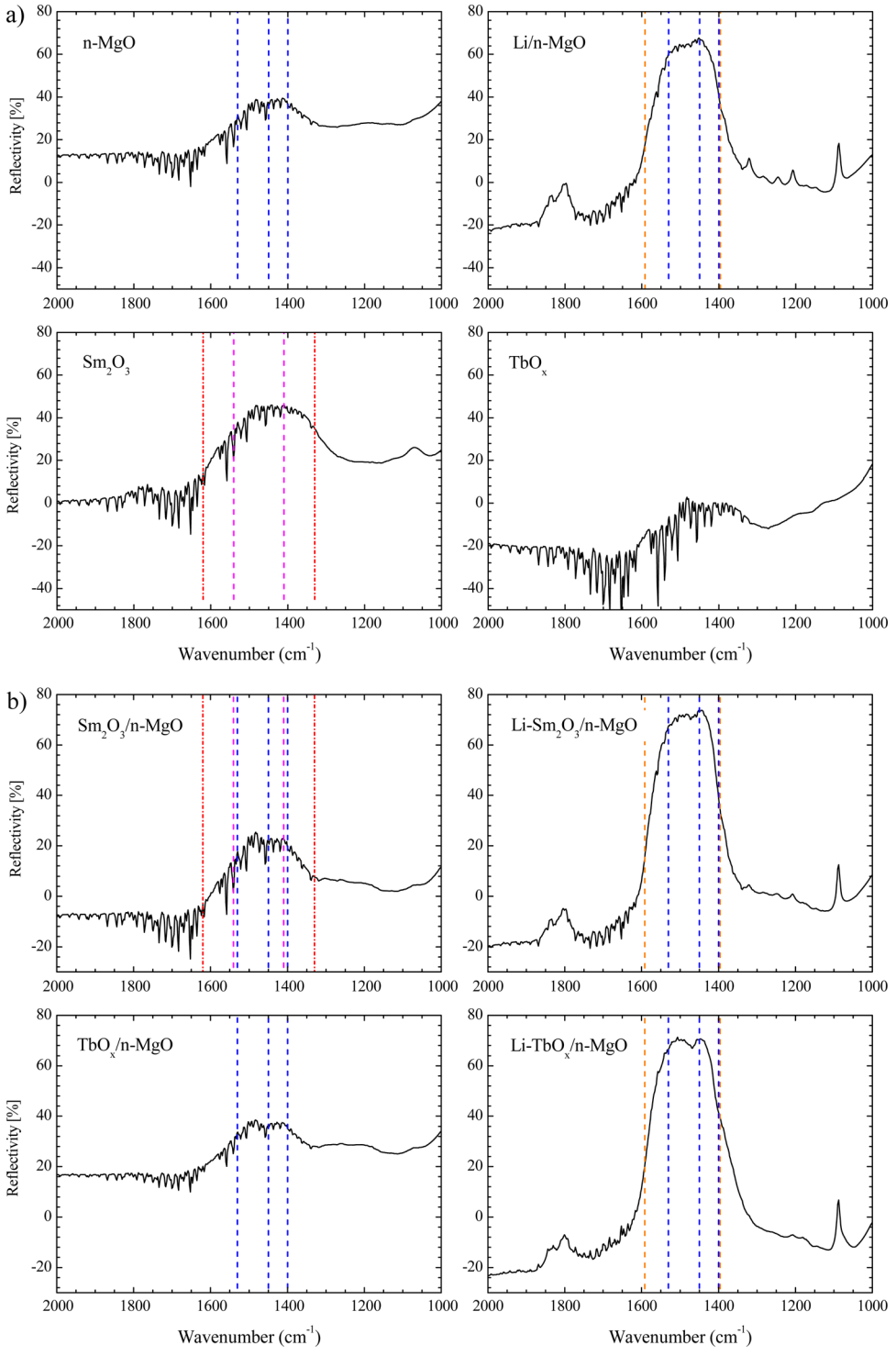

Figure 11. DRIFTS background spectra collected after outgassing at 450 °C for reference compounds and lithium-doped and undoped REO/n-MgO. Dashed lines mark positions for different carbonate species: blue dashed line, monodentate carbonates on MgO; orange dashed line, monodentate carbonate interactions with Li species;[48] red dotted/dashed line, bidentate carbonates on Sm_2O_3; and pink dashed line, monodentate carbonates on Sm_2O_3.[46]

catalysts, the n-MgO support, the Li/n-MgO catalyst, and two pure samaria and terbia nanoparticle (NP) samples (prepared using the microemulsion method) (Figures 11−13. The nature of the surface sites are important because surface oxygen is responsible for the hydrogen abstraction from methane, the key step of the OCM reaction.[2] The properties of the surface oxygen species are also important because they can react with the methyl radicals or the C_{2+} products and form surface methoxy species, which in turn can undergo oxidation to CO and CO_2.

The CO_2 molecules interact with the surface oxide and hydroxide sites to form carbonate and bicarbonate species, respectively. In-depth analysis of the DRIFTS spectra enables us to distinguish between different types of surface oxygens.[46]

dx.doi.org/10.1021/cs500138j | ACS Catal. 2014, 4, 1972−1990

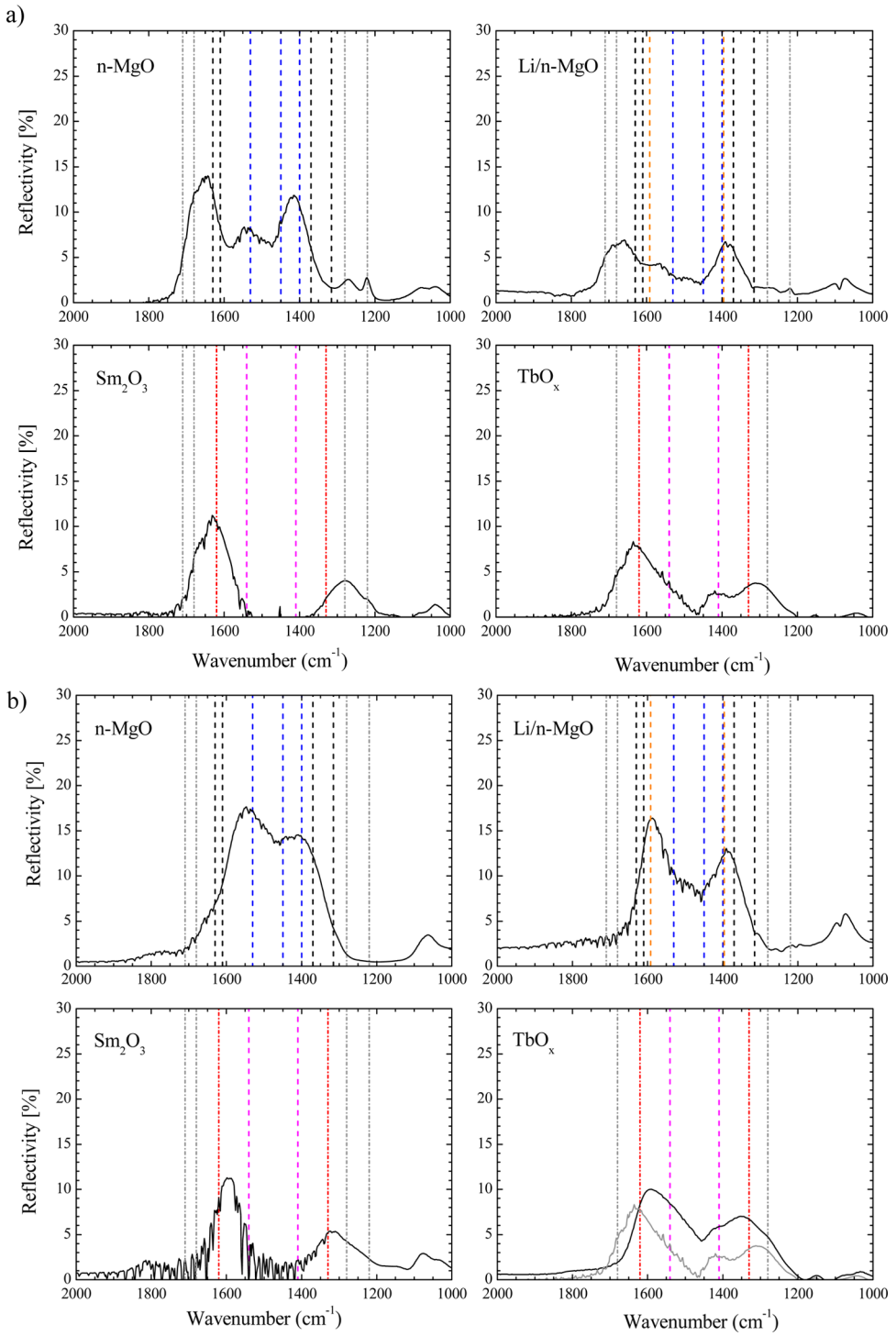

Figure 12. DRIFTS data obtained from n-MgO, Li/n-MgO as well as Sm_2O_3 and TbO_x nanoparticles after CO_2 adsorption at (a) 50 and (b) 250 °C. Solid gray line in part b is the DRIFTS data obtained after CO_2 exposure at 50 °C. The dashed vertical lines indicate the following: (black) bidentate carbonates on MgO, (blue) monodentate carbonates on MgO, (gray dotted/dashed) bicarbonates on MgO, (red dotted/dashed) bidentate carbonates on Sm_2O_3, and (pink) monodentate carbonates on Sm_2O_3,[46] and (orange) carbonate interactions with Li species.[48]

At least four types of surface oxygens have been shown to exist on the surface of magnesia, and these sites result in different carbonate species.[47] The two main types of carbonates, bidentate and monodentate carbonates, are present in the 1700−1200 cm^{-1} region as a result of CO_2 interaction with basic oxygen sites. The features in this region are due to bond-stretching carbonyl (C═O) vibrations of the different carbonate structures.

3.3.6.1. Background Spectra. Because the maximum temperature of the heating mantle used in the DRIFTS experiments is 450 °C, it is expected that most, if not all, of the adsorbed CO_2 will be removed from the TbO_x/n-MgO and Sm_2O_3/n-MgO catalyst, and most of the adsorbed CO_2 will remain on the Li-TbO_x/n-MgO and Li-Sm_2O_3/n-MgO catalysts after the 450 °C outgassing procedure. Because the surface after outgassing at 450 °C for 30 min is used to remove

dx.doi.org/10.1021/cs500138j | ACS Catal. 2014, 4, 1972−1990

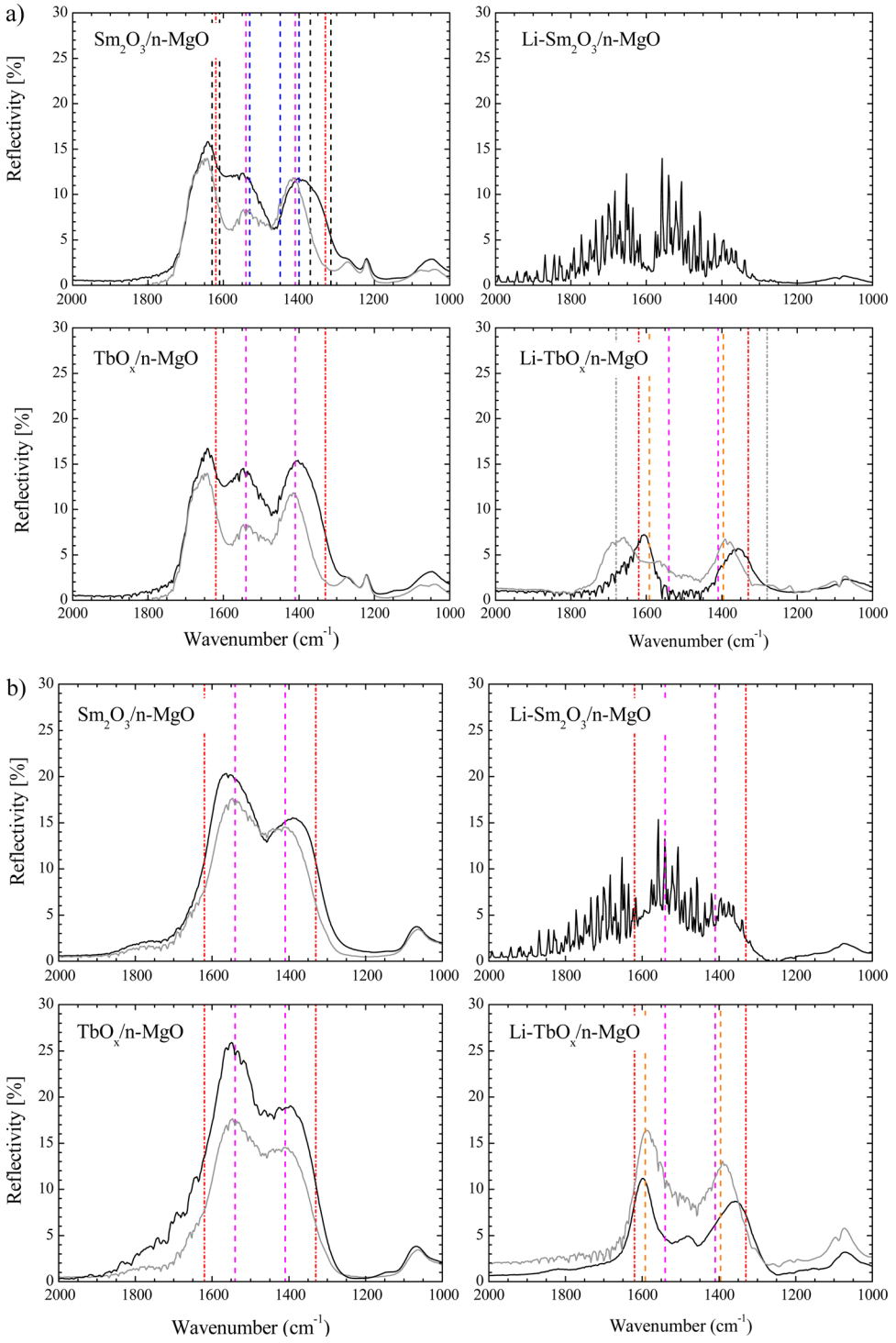

Figure 13. DRIFTS data obtained from Sm_2O_3/n-MgO, Li-Sm_2O_3/n-MgO, TbO_x/n-MgO, and Li-TbO_x/n-MgO catalysts after CO_2 adsorption at (a) 50 and (b) 250 °C. Solid black spectra lines are for the REO/n-MgO samples, and the lighter gray lines shows either the n-MgO support DRIFTS information or the Li-MgO DRIFTS spectra that the catalyst matches. The dashed vertical lines indicate the following: (black) bidentate carbonates on MgO, (blue) monodentate carbonates on MgO, (gray dotted/dashed) bicarbonates on MgO, (red dotted/dashed) bidentate carbonates on Sm_2O_3, (pink) monodentate carbonates on Sm_2O_3,[46] and (orange) carbonate interactions with Li species.[48]

background adsorption in the DRIFTS analysis, these spectra with a KBr background subtraction are shown in Figure 11. The amount of CO_2 remaining on the surface of the n-MgO support after outgassing is very low, and the same is true for the TbO_x nanoparticles, as is evident in Figure 11. In contrast, some CO_2 remains on the surface of Sm_2O_3 nanoparticles, and a significant amount of CO_2 is present on the Li/n-MgO catalyst after heat treatment at 450 °C. This suggests that the surfaces of the n-MgO support and the TbO_x NPs do not have a significant amount of highly basic sites capable of strongly binding CO_2. The Sm_2O_3 NPs are more basic than the TbO_x NPs and the n-MgO support, and the broad peaks reveal that both monodentate and bidentate carbonates are present on the surface. Compared with the Sm_2O_3 NPs, more CO_2 is bound to

dx.doi.org/10.1021/cs500138j | ACS Catal. 2014, 4, 1972−1990

the surface of the Li/n-MgO, and the majority of the species on the surface are monodentate carbonates associated with the lithium.[48]

The DRIFTS spectra with a KBr background subtraction obtained from the REO/n-MgO and Li-REO/n-MgO catalysts after heat treatment at 450 °C are also shown in Figure 11. The spectra from the Sm_2O_3/n-MgO and TbO_x/n-MgO catalysts are similar and resemble the spectra obtained from the pure n-MgO support. Thus, the amount of CO_2 remaining on the surface after outgassing at 450 °C for 30 min is very similar on these catalysts and appears to be mainly due to the support. In contrast, both Li-doped REO/n-MgO catalysts have a significant amount of carbonates present on the surface after the heat treatment. This reveals strongly bound CO_2 on the Li-containing Sm_2O_3/n-MgO and TbO_x/n-MgO catalysts, which is consistent with the TPD data (and the XPS measurements). The amount of CO_2 on the surface of these catalysts is higher than on the surface of the Li/n-MgO, but the carbonate species appear to be the same, that is, mainly monodentate lithium carbonates. The DRIFTS data not only confirm that CO_2 is strongly bound on Li-containing catalysts, it also corroborate that a temperature of 450 °C is sufficient to remove most of the CO_2 adsorbed on the TbO_x/n-MgO and Sm_2O_3/n-MgO catalysts.

The spectra in Figure 11 are used to remove the background in the DRIFTS data obtained from each of the various catalysts and reference samples after CO_2 dosing at 50 and 250 °C.

3.3.6.1. Pure and Reference Components. Results of the DRIFTS experiments on the n-MgO support, the Li/n-MgO sample, and the two Sm_2O_3 and TbO_x NP catalysts are shown in Figure 12. The DRIFTS spectrum obtained from the magnesia support after CO_2 adsorption at 50 °C is the most complex of the pure component spectra (Figure 12a), as would be expected becaue it is known to have several different basic sites.[46] In fact, all four carbonate species identified by Davydov and co-workers[46]—bicarbonate, monodentate carbonate, and two (asymmetric and symmetric) bidentate carbonates—are present after CO_2 adsorption at 50 °C (Figure 12a). Evidently, all these species are relatively weakly bound, as most of them would be removed below 500 °C, according to the TPD measurements. Carbon dioxide adsorption at 50 °C on the Li/n-MgO sample results in both bidentate carbonates and bicarbonates, in addition to the monodentate carbonates that were already present on the surface after outgassing (Figure 11). Comparing the n-MgO support and the Li/n-MgO, the n-MgO support has a higher contribution from bidentate carbonates and bicarbonates, and the monodentate carbonates dominate on the Li/n-MgO.

CO_2 adsorption on the Sm_2O_3 NPs does not increase the concentration of monodentate carbonate species; only bidentate and bicarbonate species are increased after the CO_2 dose at 50 °C (Figure 12). On the TbO_x NPs that had very little CO_2 on the surface after the outgassing procedure, a small amount of monodentate carbonates together with bidentate carbonates and bicarbonates are present after the CO_2 exposure. The wavenumbers of the carbonates are close to those obtained from the reference values for carbonates on Sm_2O_3. The relative peak heights reveal that the concentration of bidentate carbonates is higher than the concentration of monodentate carbonates on the pure terbia nanoparticles.

As the temperature of the CO_2 dosing is increased to 250 °C, a smaller amount of bidentate carbonate species is present on the surface, the bicarbonate species are removed, and the concentration of monodentate species is significantly increased on the pure n-MgO support surface (Figures 12a,b). Because the Li/n-MgO sample already has a large number of monodentate species on the surface (higher than the amount observed on the n-MgO after the 250 °C exposure), mainly the bidentate carbonate species increase after the 250 °C CO_2 exposure. There are also new carbonate peaks on the catalyst's surface after doping with lithium. These peaks are most likely due to carbonates chemisorbed on lithium because the peaks match well with data obtained on a lithium-doped Al_2O_3-MgO catalyst system.[48]

As for the n-MgO support, a temperature of 250 °C appears to be sufficient to remove the bicarbonates and yield more strongly bound mono- and bidentate carbonate species. In both cases, the amount of CO_2 adsorbed on the surface is higher at 250 °C compared with adsorption at 50 °C. Some of the bicarbonate species are removed after the 250 °C exposure also on the TbO_x and Sm_2O_3 NPs, but only on the TbO_x NPs is there a slight increase in the mono- and bidentate carbonate species compared with the 50 °C exposure. It appears that the amount of CO_2 adsorbed on the Sm_2O_3 NPs at 250 °C is smaller than the amount present after dosing at 50 °C. In contrast, the n-MgO, Li/n-MgO, and TbO_x all have more CO_2 adsorbed on surface after CO_2 exposure at the higher temperature.

3.3.6.2. Sm_2O_3/n-MgO and TbO_x/n-MgO Catalysts. Consistent with the data obtained after outgassing at 450 °C (Figure 11), the DRIFTS spectra obtained from the Sm_2O_3/n-MgO and TbO_x/n-MgO catalysts are dominated by CO_2 adsorbed on the MgO support (Figure 13); however, compared with the IR spectra obtained from the pure MgO support, more CO_2 is adsorbed on the REO/n-MgO catalysts (compare Figures 12 and 13). More mono- and bidentate carbonate species are observed on the surfaces of the Sm_2O_3/n-MgO and TbO_x/n-MgO catalysts, compared with the n-MgO after CO_2 exposure at 50 °C. Because the CO_2 adsorption is dominated by the n-MgO support, the IR spectra obtained from the Sm_2O_3/n-MgO and TbO_x/n-MgO catalysts are very similar, despite the differences in the CO_2 adsorption on the Sm_2O_3 and TbO_x NPs. Thus, on the supported catalysts, the concentration of monodentate carbonates is higher than on any of the pure components.

At a CO_2 adsorption temperature of 250 °C, the spectra obtained from both the Sm_2O_3/n-MgO and TbO_x/n-MgO catalysts more closely resemble the spectrum obtained from n-MgO compared with the data obtained after dosing at 50 °C (Figure13a,b). This is due to the fact that the main species on the surfaces of the n-MgO support and the REO/n-MgO catalysts after this exposure are monodentate carbonates. The main difference between the supports and the catalysts is that the signal intensity is higher on the catalysts, that is, more monodentate carbonates are present on the REO/n-MgO catalysts compared with the n-MgO support. It appears that slightly more CO_2 is adsorbed on the TbO_x/n-MgO catalyst compared with the Sm_2O_3/n-MgO catalyst; however, quantification is difficult because the CO_2 remaining on the surface after outgassing is marginally higher on the Sm_2O_3/n-MgO catalyst compared with the TbO_x/n-MgO catalyst.

3.3.6.3. Li-Sm_2O_3/n-MgO and Li-TbO_x/n-MgO Catalysts. Adding Li to Sm_2O_3/n-MgO and TbO_x/n-MgO catalysts results in a significant increase in the strongly bound CO_2 on the surface, as evident in Figure 11. Considering the amount of CO_2 present on the surface in the form of monodentates, it is

dx.doi.org/10.1021/cs500138j | ACS Catal. 2014, 4, 1972−1990

not surprising that the CO_2 uptake on the Li-REO/n-MgO catalysts is low (Figure 13). It appears that the surface is almost saturated because very little CO_2 can be added to the Li-Sm_2O_3/n-MgO, irrespective of the dosing temperature (Figure 13a,b). In contrast, some bidentate carbonates are present on the surface of the Li-TbO_x/n-MgO catalyst after dosing CO_2 at 50 °C. Increasing the dosing temperature to 250 °C increases both the monodentate and the bidentate carbonate concentrations on this catalyst.

4. CONCLUSION

The reaction data obtained in this study reveal that coimpregnating lithium and a terbia precursor yields a catalyst that is highly active and selective in the oxidative coupling of methane, despite the fact that terbia itself is not a selective OCM catalyst. Addition of Li more than doubled the C_{2+} yield of the TbO_x/n-MgO catalysts, regardless of preparation method, and the lithium nitrate precursor consistently gave a higher C_{2+} selectivity compared with the lithium carbonate precursor. This increase in C_{2+} yield with Li addition is due to both an increase in methane conversion and an appreciably higher C_{2+} selectivity (TbO_x is typically highly selective to CO and CO_2). The Li-TbO_x/n-MgO also exhibit a lower activity loss with time on-stream compared with both Li/n-MgO and Li-Sm_2O_3/n-MgO catalysts. In fact, the Li-TbO_x/n-MgO catalyst exhibited less deactivation after 30 h on-stream than the Li/MgO after just 8 h on-stream under the same conditions. Furthermore, the Li-TbO_x/n-MgO catalyst is highly active and selective at a temperature as low as 650 °C. The lower OCM reaction temperature is an important factor in the application toward an industrial process. Addition of Li to the Sm_2O_3/n-MgO also increased the C_{2+} yield, but the activity loss is higher and temperature-dependent for this catalyst.

Li induces reduction of the TbO_x phase to Tb_2O_3, as evidenced by both XRD and XPS, which is likely more active toward C_{2+} products than the TbO_x. Addition of Li also shifts the Tb 3d core-level electrons to higher binding energies, which is another indication of strong Li-TbO_x interactions. This, in turn, could explain the higher stability of the Li-TbO_x/n-MgO compared with the other Li-containing catalysts. For both the Sm_2O_3/n-MgO and the TbO_x/n-MgO catalysts, addition of Li increased the number and strength of the basic sites. More CO_2 adsorption is observed on the Li-doped REO/n-MgO catalysts, and the binding strength of the CO_2 is higher compared with the undoped catalysts. These highly basic sites may be required for the hydrogen abstraction from methane to initiate the coupling reaction. Although the activity and stability of the Li-TbO_x/n-MgO catalyst system is lower than the Mn-Na_2WO_4/SiO_2 catalyst, the potential benefit of using the Li-TbO_x/n-MgO catalyst is the lower reaction temperature (600−700 °C versus 800−875 °C for the Mn-Na_2WO_4/SiO_2 system). Future work on this system is therefore focused on utilizing other alkali or alkali earth metals to address the issue of lithium volatilization and find a more stable REO-based catalyst.

AUTHOR INFORMATION

Corresponding Author

*Phone: 352-392-6585. E-mail: hweaver@che.ufl.edu.

Notes

The authors declare no competing financial interest.

ACKNOWLEDGMENTS

The authors gratefully acknowledge NSF support (Chemistry 1026712). Dr. Valentin Craciun, Dr. Eric Lambers, and Mr. Gill Brubaker are acknowledged for the analytical equipment training and technical assistance during XRD, XPS, and BET surface area measurements. These analyses were performed at the Major Analytical Instrumentation Center (MAIC) and the Particle Engineering Research Center (PERC) at the University of Florida (UF). Dr. Volkmar Zielasek (IAPC) and Dr. Johannes Birkenstock (Geoscience Department) are gratefully acknowledged for their assistance in collecting the TEM and XRD data, and Dr. Kari Basso (UF Chemistry mass spectrometry services), for assistance with MS analysis of the condensate. We are also thankful for Mr. Xianhe Deng's assistance during the 30-h reaction experiment.

REFERENCES

(1) Keller, G. E.; Bhasin, M. M. *J. Catal.* **1982**, *73*, 9−19.
(2) Ito, T.; J. Wang, J.; Lin, C.; Lunsford, J. H. *J. Am. Chem. Soc.* **1985**, *107*, 5062−5068.
(3) Driscoll, D. J.; Martir, W.; Wang, W.; Lunsford, J. H. *J. Am. Chem. Soc.* **1985**, *107*, 58−63.
(4) Arndt, S.; Simon, U.; Heitz, S.; Berthold, A.; Beck, B.; Görke, O.; Epping, J. D.; Otremba, T.; Aksu, Y.; Irran, E.; Laugel, G.; Driess, M.; Schubert, H.; Schomäcker, R. *Top. Catal.* **2011**, *54*, 1266−1285.
(5) Mirodatos, C.; Perrichon, V.; Durupty, M. C.; Moral, P. *Stud. Surf. Sci. Catal.* **1987**, *34*, 183−195.
(6) Korf, S. J.; Roos, J. A.; de Brujin, N. A.; van Ommen, J. G.; Ross, J. R. H. *Catal. Today* **1988**, *2*, 535−545.
(7) Tang, L.; Yamaguchi, D.; Wong, L.; Burke, N.; Chiang, K. *Catal. Today* **2011**, *178*, 172−180.
(8) Simon, U.; Arndt, S.; Otremba, T.; Schlingmann, T.; Görke, O.; Dinse, K. P. *Catal. Commun.* **2012**, *18*, 132−136.
(9) Langfeld, K.; Frank, B.; Strempel, V. E.; Berger-Karin, C.; Weinberg, G.; Kondratenko, E. V.; Schomäcker, R. *Appl. Catal., A* **2012**, *417−418*, 145−152.
(10) Wang, D.; Rosynek, M. P.; Lunsford, J. H. *J. Catal.* **1995**, *151*, 155−167.
(11) Campbell, K. D.; Lunsford, J. H. *J. Phys. Chem.* **1988**, *92*, 5792−5796.
(12) Maksimov, N. G.; Selyutin, G. E.; Anshits, A. G.; Kondratenko, E. V.; Roguleva, V. G. *Catal. Today* **1998**, *42*, 279−281.
(13) Leveles, L.; Fuchs, S.; Seshan, K.; Lercher, J. A.; Lefferts, L. *Appl. Catal., A* **2002**, *227*, 287−297.
(14) Spinicci, R.; Marini, P.; De Rossi, S.; Faticanti, M.; Porta, P. *J. Mol. Catal. A: Chem.* **2001**, *176*, 253−265.
(15) Machocki, A.; Jezior, R. *Chem. Eng. J.* **2008**, *137*, 643−652.
(16) Otsuka, K.; Jinno, K.; Morkawa, A. *J. Catal.* **1986**, *100*, 353−359.
(17) Forlani, O.; Rossini, S. *Mater. Chem. Phys.* **1992**, *31*, 155−158.
(18) Zhang, H. B.; Lin, G. D.; Wan, H. L.; Liu, Y. D.; Weng, W. Z.; Cai, J. X.; Shen, Y. F.; Tsai, K. R. *Catal. Lett.* **2001**, *73*, 141−147.
(19) Vereshchagin, S. N.; Ross, J. R. H. *Catal. Today* **1995**, *24*, 285−287.
(20) Al-Zahrani, S. M.; Elbashir, N. O.; Abasaeed, A. E.; Abdulwahed, M. *J. Mol. Catal. A: Chem.* **2004**, *218*, 179−186.
(21) Neumann, B.; Elkins, T. W.; Dreher, W.; Hagelin-Weaver, H.; Nino, J. C.; Bäumer, M. *Catal. Sci. Technol.* **2012**, *3*, 89−93.
(22) Campbell, K. D.; Zhang, H.; Lunsford, J. H. *J. Phys. Chem.* **1988**, *92*, 750−753.
(23) Dedov, A. G.; Loktev, A. S.; Moiseev, I. I.; Aboukais, A.; Lamonier, J. F.; Filimonov, I. N. *Appl. Catal., A* **2003**, *245*, 209−220.
(24) Deboy, J. M.; Hicks, R. F. *J. Catal.* **1988**, *113*, 517−524.
(25) Elkins, T. W.; Hagelin-Weaver, H. E. *Appl. Catal., A* **2013**, *454*, 100−114.
(26) Korf, S. J.; Roos, J. A.; Diphoorn, J. M.; J. Veehof, R. H.; van Ommen, J. G.; Ross, J. R. H. *Catal. Today* **1989**, *4*, 279−292.

(27) Gaffney, A. M.; Jones, C. A.; Leonard, J. J.; Sofranko, J. A. *J. Catal.* **1988**, *114*, 422−432.
(28) Simon, U.; Görke, O.; Berthold, A.; Arndt, S.; Schomäcker, R.; Schubert, H. *Chem. Eng. J.* **2011**, *168*, 1352−1359.
(29) Pak, S.; Qiu, P.; Lunsford, J. H. *J. Catal.* **1998**, *179*, 222−230.
(30) Kiu, H. T.; Wang, X. L.; Yang, D. X.; Gao, R. X.; Wang, Z. L.; Yang, J. *J. Nat. Gas Chem.* **2008**, *17*, 59−63.
(31) Arndt, S.; Otremba, T.; Simon, U.; Yildiz, M.; Schubert, H.; Schomacker, R. *Appl. Catal., A* **2012**, *425*−*426*, 53−61.
(32) Yu, Z. Q.; Yang, X. M.; Lunsford, J. H.; Rosynek, M. P. *J. Catal.* **1995**, *154*, 163−173.
(33) Hutchings, G. J.; Scurrel, M. S.; Woodhouse, J. R. *Catal. Today* **1989**, *4*, 371−381.
(34) NanoScale Materials Inc.: http://nanoactive.interkan.net/content/nanoactive_materials/nanoactive_home.asp, accessed on 10/01/2008.
(35) Gilbert, R. E.; Cox, D. F.; Hoflund, G. B. *Rev. Sci. Instrum.* **1982**, *53*, 1281−1284.
(36) Moulder, J. F.; Stickle, W. F.; Sobol, P. E.; Bomben, K. D. In *Handbook of X-ray Photoelectron Spectroscopy*, 2nd ed.; Chastain, J., King, R. C. Jr., Eds.; Physical Electronics Inc.: Eden Prairie, MN, 1995.
(37) Wan, H. L.; Zhou, X. P.; Weng, W. Z.; Long, R. Q.; Chao, Z. S.; Zhang, W. D.; Chen, M. S.; Luo, J. Z.; Zhou, S. Q. *Catal. Today* **1999**, *51*, 161−175.
(38) Choudhary, V. R.; Mulla, S. A. R.; Rane, V. H. *J. Chem. Technol. Biotechnol.* **1998**, *71*, 167−172.
(39) Farsi, A.; Moradi, A.; Ghader, S.; Shadravan, V. *Chin. J. Chem. Phys.* **2011**, *24*, 70−76.
(40) Jeon, W.; Lee, J. Y.; Leea, M.; Choi, J.-W.; Haa, J.-M.; Suha, D. J.; Kim, I. W. *Appl. Catal., A* **2013**, *464*−*465*, 68−77.
(41) Papa, F.; Luminita, P.; Osiceanu, P.; Birjega, R.; Akane, M.; Balint, I. *J. Mol. Catal. A: Chem.* **2011**, *346*, 46−54.
(42) Aritani, H.; Yamada, H.; Nishio, T.; Imamura, S.; Hasegawa, S.; Tanaka, T.; Yoshida, S. *Chem. Lett.* **1999**, *28*, 359−360.
(43) Aritani, H.; Yamada, H.; Nishio, T.; Shiono, T.; Imamura, S.; Kudo, M.; Hasegawa, S.; Tanaka, T.; Yoshida, S. *J. Phys. Chem. B* **2000**, *104*, 10133−10143.
(44) Esquivel, M. R.; Bohé, A. E.; Pasquevich, D. M. *Mater. Res. Bull.* **2007**, *42*, 553−562.
(45) NIST Standard X-ray Photoelectron Spectroscopy Reference Database 20, Version 4.1; http://srdata.nist.gov/xps/, accessed on 12/16/2013.
(46) Davydov, A. In *Molecular Spectroscopy of Oxide Catalyst Surfaces*, 1st ed.; Sheppard, N. T., Ed.; John Wiley & Sons Ltd: Chichester, 2003.
(47) Davydov, A. A. *Chem. Eng. Technol.* **1995**, *18*, 7−11.
(48) Escobar-Alarcon, L.; Klimova, T.; Escobar-Aguilar, J.; Romero, S.; Morales-Ramirez, C.; Solis-Casados, D. *Fuel* **2013**, *110*, 278−285.